UNIVERSITY OF THE
FREE STATE
UNIVERSITEIT VAN DIE
VRYSTAAT
YUNIVESITHI YA
FREISTATA

UFS
UV

Establishing a doxorubicin-resistant triple-negative breast cancer spheroid model

by

VIWE FOKAZI

(2019374566)

Submitted in fulfilment of the requirements for the degree of Master of Medical Science (Pharmacology)

in the

Department of Pharmacology

Faculty of Health Sciences

University of the Free State

Supervisor: Prof Mamello Sekhoacha

Co-supervisors: Prof Chrisna Gouws and Dr Beynon Abrahams

30 July 2024

DECLARATION

I, Viwe Fokazi, declare that the Master's Degree research dissertation that I herewith submit for the Master's Degree with specialisation in pharmacology at the University of the Free State is my independent work and that I have not previously submitted it for a qualification at another institution of higher education.

Viwe Fokazi	22 July 2024
Name and Surname	Date

DEDICATION

I WOULD LIKE TO DEDICATE THIS DEGREE TO MY LATE SISTER (ZINTLE KWEZA), WHO SAW ME START THIS JOURNEY BUT UNFORTUNATELY COULDN'T SEE ME FINISH IT. I KNOW YOU WOULD BE CHEERING ME ON.

I WOULD ALSO LIKE TO DEDICATE THIS DEGREE TO MYSELF FOR PUTTING IN THE HARD WORK AND FOR OVERCOMING EVERY CHALLENGE I FACED.

SUPERVISOR DECLARATION

UNIVERSITY OF THE FREE STATE
UNIVERSITEIT VAN DIE VRYSTAAT
YUNIVESITHI YA FREISTATA

UFS·UV
HEALTH SCIENCES
GESONDHEIDSWETENSKAPPE

Department of Pharmacology

22 July 2024

Postgraduate Office
Faculty of Health Science
University of the Free State
Bloemfontein 9300

Regarding Viwe Fokazi's submission of a master's dissertation for examination: Supervisor's declaration

I, Professor Mamello Sekhoacha, the supervisor of the master's research dissertation entitled: **Establishing A Doxorubicin-Resistant Triple-Negative Breast Cancer Spheroid Model**, hereby certify that the work in this project was done by Viwe Fokazi (student number: 2019374566) registered at the Department of Pharmacology, University of the Free State. I hereby approve the submission of this thesis and affirm that this has not been submitted previously, either in part or in its entirety, to the assessors, neither to this or any other institution foradmission to a degree or any other qualification.

Date .....22 July 2024..... Signature ....

TABLE OF CONTENTS

ACKNOWLEDGEMENTS

To God: "*I will lift up my eyes to the hills – from whence comes my help? My help comes from the Lord, who made heaven and earth".* You have held my hand throughout this journey, walked with me, carried me, walked before me and levelled every mountain, and most of all, been my pillar of strength. I am grateful.

To my supervisors, Prof MP Sekhoacha, Dr B Abrahams and Prof C Gouws: I want to express my deepest gratitude for the dedication and effort you have all invested in making my dissertation what it is. Your willingness to go above and beyond whenever I needed assistance has been invaluable. Thank you for your unwavering support, patience, and compassion throughout this process. I am especially grateful for your belief in me and the continual affirmation of my academic potential. I will carry the lessons and invaluable advice you have shared with me throughout this journey into all aspects of my life.

To Dr Alandi: Thank you for being an exceptional teacher! I am deeply grateful for the warmth and kindness with which you welcomed us. Your dedication to helping us was evident in your constant willingness to support us and your consistent presence whenever we needed assistance. Your patience and the skills you imparted have been invaluable. Thank you for your unwavering commitment and for making such a significant impact on our learning experience.

To Dr Joshua: Thank you so much for your assistance with referencing and dissertation edits.

To my mother: Thank you for your unwavering support and encouragement. I am deeply grateful for your prayers and for helping me navigate the challenges and mini-breakdowns I faced. Your emotional support has been a pillar of strength for me, and I sincerely appreciate it.

To my lab partner and friend, O Ngalonkulu: We made an excellent team, and I'm truly grateful to have shared this journey with you. Although it wasn't an easy path, we supported each other every step of the way. We shared both tears and laughter, and our

post-lab outings were the perfect way to unwind after our long and exhausting days. I cherish the time we spent together and the bond we built.

To my funders: Thank you to the UFS postgrad bursary and the National Research Fund for providing me with funding**.**

RESEARCH OUTPUTS

Poster presentations

1. Fokazi V; Sekhoacha MP; Abrahams BR; Gouws C. Establishing a doxorubicin-resistant triple-negative breast cancer spheroid model. Society for Advanced Cell Culture Modelling for Africa (SACCMA), Potchefstroom, South Africa, 10 October 2022.
2. Fokazi V; Sekhoacha MP; Abrahams BR; Gouws C. Establishing a doxorubicin-resistant triple-negative breast cancer spheroid model. The 3rd Microphysiological Systems World Summit, Seattle, United States of America, 11 June 2024.

LIST OF FIGURES

LIST OF TABLES

LIST OF ABBREVIATIONS

2D	Two-dimensional
3D	Three-dimensional
ABC	ATP-binding cassette
ADP	Adenosine diphosphate
AK	Adenylate kinase
AMP	Adenosine monophosphate
ANOVA	Analysis of variance
ATCC	American Tissue Culture Collection
ATP	Adenosine triphosphate
BC	Breast cancer
BCRP	Breast cancer-resistant protein
BL	Basal-like
BLIS	Basal-like and immune-suppressed
BM	Basement membrane
BRCA1	Breast cancer susceptibility gene 1
BRCA2	Breast cancer susceptibility gene 2
BSA	Bovine serum albumin
BSE	Breast self-examination
CBE	Clinical breast examination
CICs	Cell-in-cell structures
CSCs	Cancer stem cells
DMEM	Dulbecco's modified essential medium
DNA	Deoxyribonucleic acid
DMSO	Dimethyl sulfoxide

DoxR	Doxorubicin-resistant
ECM	Extracellular matrix
EGFR	Epidermal growth factor receptor
EMT	Epithelial-mesenchymal transition
ER	Estrogen receptor
FBS	Foetal bovine serum
FGF	Fibroblast growth factor
FU	Fluorouracil
h	hour(s)
HBOC	Hereditary breast/ovarian cancer
HCl	Hydrochloric acid
HEPA	High-efficiency particulate air
HER-2	Human epidermal growth factor receptor 2
Hh	Hedgehog
HR	Hormone receptor
HRT	Hormone replacement therapy
IBC	Inflammatory breast cancer
IM	Immunomodulatory
IM	Interstitial membrane
LAR	Luminal androgen receptor
MDR	Multidrug resistance
MES	Mesenchymal-like
MMPs	Metalloproteinases
mRNA	messenger ribonucleic acid
MRI	Magnetic resonance imaging

MRP	Multidrug-resistant protein
mTOR	Mammalian target of rapamycin
O_2	Oxygen
OD	Optical density
P-gp	P-glycoprotein
PBS	Phosphate-buffered saline
PCL	Polycaprolactone
pCR	Pathologic complete response
PEG	Polyethylene glycol
PI3Ks	Phosphoinositide 3-kinases
PLGA	Polylactic-co-glycolic acid
PR	Progesterone receptor
Prot	Protein
R	Radius of the spheroid
ROS	Reactive oxygen species
RPM	Rotations per minute
SOC	Standard of care
SRB	Sulforhodamine B
TME	Tumour microenvironment
TNBC	Triple-negative breast cancer
TILs	Tumours infiltrating lymphocytes
VEGF	Vascular endothelial growth factor
WHO	World Health Organization
Wnt	Wingless-related integration site

ABSTRACT

Introduction: Triple-negative breast cancer (TNBC) is the most lethal subtype of breast cancer. Cytotoxic chemotherapy and immune therapy remain the only available therapeutic strategies for treatment, but unfortunately, patients frequently develop resistance. Resistance to chemotherapeutic agents is a major obstacle to effective cancer treatment. Two-dimensional (2D) cell-based models are conventionally used for the *in vitro* screening of anti-cancer compound activity. However, these models do not accurately represent the complexities associated with the tumour microenvironment, thus limiting the reliability of research results. **Aim:** This project aimed to develop, characterise and qualify a novel three-dimensional (3D) doxorubicin-resistant MDA-MB-231 TNBC spheroid model using a clinostat-based rotating bioreactor, which more closely represents the *in vivo* environment to study drug activity and drug resistance. **Method:** The 3D doxorubicin-resistant MDA-MB-231 TNBC spheroid model was characterised over 27 days, based on the following parameters: planimetric analysis; soluble protein content; intracellular adenosine triphosphate (ATP); extracellular adenylate kinase (AK); and approximate glucose consumption assays. Data obtained from the characterisation was used to determine the metabolically stable experimental treatment period of the spheroids. Qualification of the spheroid model was conducted using clinical dosing with cisplatin and doxorubicin over a 96-hour treatment period. **Results:** An MDA-MB-231 TNBC spheroid model was successfully developed and characterised. The model was viable and maintained its structure until day 27. The experimental window was determined to be between days 15 and 23, during which validation was conducted. The model was highly responsive to both cisplatin and doxorubicin treatment. **Conclusion:** Since the established model was responsive to both chemotherapeutic treatments, its application in evaluating drug resistance appeared limited. This model may, however, still provide benefits as a chemo-sensitive advanced TNBC breast cancer cell model for screening novel compounds for potential anti-cancer activity.

Keywords: triple-negative breast cancer; two-dimensional cell culture; three-dimensional cell culture; drug resistance; doxorubicin.

CHAPTER ONE

1.0 INTRODUCTION

1.1 BACKGROUND

Cancer results from the abnormal and uncontrolled proliferation of the body's cells. This gives rise to multiple types of cancers, each with unique behaviour and therapeutic response (Cooper and Hausman, 2000). Cancer cells consist of a set of characteristics known as the 'hallmarks' of cancer (Figure 1.1 A), which include the acquired abilities to maintain proliferative signalling; elude growth suppressors; enable replicative immortality; resist cell death; induce/access vasculature; activate invasion and metastasis; reprogramme cellular metabolism; and avoid immune devastation. These hallmarks refer to a set of functional abilities that human cells acquire as they transition from normal growth stages to neoplastic growth states and the development of malignant tumours (Hanahan, 2022). Hanahan modified the framework in 2022 and introduced four new developing hallmarks and enabling characteristics (Figure 1.1 B).

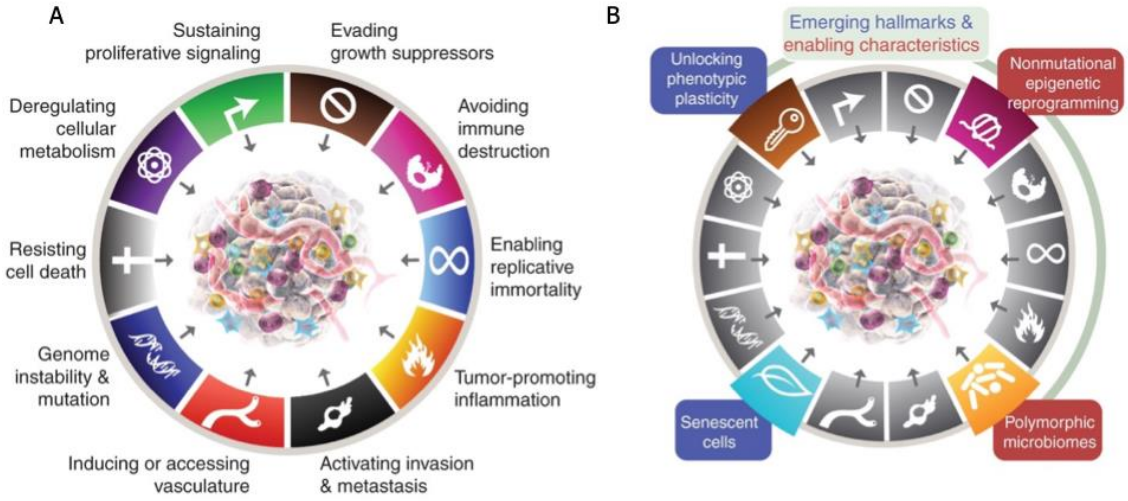

Figure 1.1: (A): hallmarks of cancer. (B): proposed new developing hallmarks and enabling characteristics involving 'unlocking phenotypic plasticity, non-mutational epigenetic reprogramming, polymorphic microbiomes, and senescent cells' (Hanahan, 2022).

Cancer can develop in different parts of the body, e.g., the brain, liver, lung, breast, prostate, cervix, ovaries, etc. It is named after the organ in which it first developed. It begins as localised to the organ and can develop a metastatic ability to spread to other parts of the body, leading to their misfunctioning. Breast, prostate, lung, and colon/rectum cancers are the four most prevalent cancer types, making up over half of all cancer cases (Cooper and Hausman, 2000).

Breast cancer has overtaken lung cancer as the most commonly diagnosed cancer in 2020, and it is among the leading cause of cancer-related deaths among women. It is responsible for 11.7% of all cancer incidents worldwide (Figure 1.2 A) (Sung et al., 2021). It is a heterogeneous group of cancers that are classified into four main types based on immunohistochemical profiles: luminal A, which is positive for oestrogen receptor (ER) and progesterone receptor (PR) but negative for human epidermal growth factor receptor (HER-2) receptor; luminal B, which is positive for ER and sometimes HER-2 but negative for PR; HER-2 positive tumours, but which are not ER or PR positive; and triple-negative breast cancer (TNBC) that is ER, PR and HER-2 negative (Figure 1.3) (Engebraaten et al., 2013). TNBC makes up 15–20% of all breast cancer cases identified each year and is more common in younger women, particularly those of African ancestry (Nedeljković and Damjanović, 2019, Firatligil-Yildirir and Yalcin-Ozuysal, 2023). TNBC lacks hormone and human epidermal growth factor receptor expression. Consequently, there are currently no known effective targeted medicines, and the main systemic therapeutic options are chemotherapy or, more recently, immunotherapy. Chemo-resistance has frequently developed in individuals who have relapsed disease following adjuvant or neo-adjuvant therapy, resulting in a poor treatment response (Abd El-Aziz et al., 2021). Drug resistance is characterised by the decrease in the effectiveness of a drug and may be presented by

local recurrence or metastasis (Alfarouk et al., 2015). Drug resistance could result from intrinsic/acquired factors or extrinsic factors. The factors associated with the evolution of both intrinsic and acquired multidrug resistance (MDR) include those that hinder the distribution of antineoplastic drugs to the tumour and reverse their cytotoxic effects, as well as those that modify the genetic or epigenetic factors of tumours, resulting in drug resistance (Saraswathy and Gong, 2013). Extrinsic factors include an altered expression of the drug's target, drug breakdown, decreased drug uptake, or enhanced drug delivery from the cell (Abd El-Aziz et al., 2021).

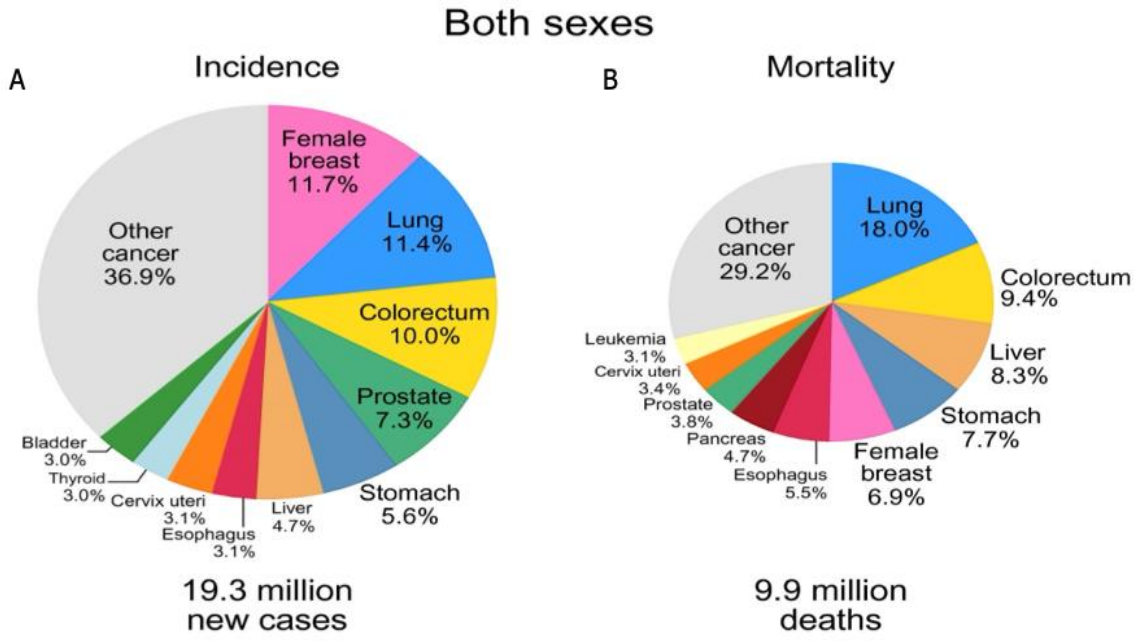

Figure 1.2: Distribution of cases and deaths for both sexes' top 10 most common cancers in 2020 (Sung et al., 2021).

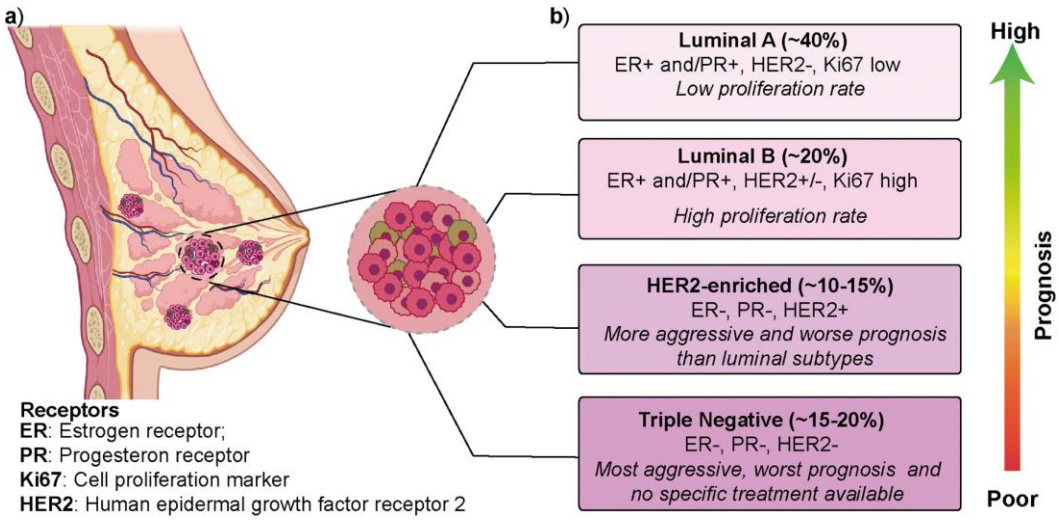

Figure 1.3: Molecular classification of breast cancer subtypes, showing their prevalence and associated hormone receptors (Firatligil-Yildirir and Yalcin-Ozuysal, 2023). Reproduced with permission from the Royal Society of Chemistry.

The occurrence and prevalence of drug resistance have led to the constant search for chemotherapeutic molecules from different sources, including natural products and combinatorial chemistry. Pre-clinical cancer research to assess the efficacy of experimental or lead therapeutics is traditionally conducted in cancer cells grown in a monolayer on a petri dish, and these cells are known as two-dimensional (2D) cultured cell models. However, these models have several limitations and thus need advanced assays and novel high throughput *in vitro* models (Nyga et al., 2011, Kapałczyńska et al., 2018). Three-dimensional (3D) cell models are cultured in an environment that permits cells to grow and interact with the adjacent extracellular framework in three dimensions. These models more closely resemble the microenvironment detected *in vivo* better than the 2D models and are thus being utilised to improve cancer drug resistance and sensitivity prediction (Ryan et al., 2016). Therefore, this study aimed to develop a 3D MDA-MB-231 TNBC-resistant cell model in the form of a spheroid and then to characterise

and qualify the model through the evaluation of its response to exposure to two selected chemotherapeutic drugs, doxorubicin and cisplatin.

1.2 PROBLEM STATEMENT

There is a major obstacle in the successful chemotherapeutic treatment of TNBC due to treatment failure associated with multidrug resistance. The current *in vitro* methods used for anti-cancer drug testing, screening and drug efficacy evaluation, including 2D cell-based models and in vivo animal models, lack adequate representation of the tumour microenvironment (TME) that mimics the environment in the living body and the genetic background in humans. The 2D cell-line-based drug efficacy assays cannot reliably predict tumour response to anti-cancer drugs as molecular pathways are not replicated in the *in vitro* flat cultures. Another limitation is that 2D cell cultures do not resemble the TME and do not accurately display cell-cell and cell-ECM interactions as in a living system. On the other hand, the use of animal models for drug screening and drug efficacy evaluation presents various shortcomings due to the physiological differences between humans and animals. The use of animal models is also of great ethical concern. There is a desperate need to establish reliable and predictive platforms to improve drug screening and drug efficacy evaluation by considering the pathophysiology of the TME. Three-dimensional *in vitro* tumour models could merge the gap between *in vitro* and *in vivo* (animal) studies, allowing for clinically relevant discoveries. Three-dimensional cell cultures involve the growth of cells as spheroids or mini tumours to more closely imitate the complexity and heterogeneity of the TME and signalling pathways used to develop multidrug resistance.

1.3 RATIONALE

Therapeutic drug resistance in breast cancer cells has been a challenge for decades. The continued high mortality rates of patients have obscured the success of current therapeutic efforts. This is partly due to the use of ineffective pre-clinical drug screening systems, such as 2D *in vitro* models, to assess drug efficacy, which does not adequately translate the TME conditions (Brancato et al., 2020). To overcome drug resistance in

TNBC, the ability to successfully model this mechanism in the laboratory is crucial (Roarty and Echeverria, 2021). Recently, a growing amount of research has suggested that 3D cell culture systems could be used to overcome the limitations of conventional drug screening and drug efficacy methods, as 3D cell-based models better replicate the actual milieu in which cells live in tissues. As a result, the activity of 3D-grown cells is more indicative of *in vivo* cellular responses to drugs (Edmondson et al., 2014). In this study, we will establish a 3D drug-resistant TNBC spheroid model. The model will be characterised and qualified.

1.4 RESEARCH QUESTION

Can an *in vitro* 3D model be used as a tool for drug-resistant TNBC treatment evaluation?

1.5 AIM

Establish, characterise and qualify a novel 3D doxorubicin-resistant MDA-MB-231 TNBC spheroid model.

1.6 OBJECTIVES

1. Induce drug resistance in 2D MDA-MB-231 TNBC cells using DOX.
2. Develop a 3D MDA-MB-231 TNBC drug-resistant spheroid model using a ClinoStar™ rotating bioreactor system.
3. Characterise the viability and growth of the 3D MDA-MB-231 TNBC spheroid model, in terms of planimetry; soluble protein content; approximate glucose uptake; extracellular adenylate kinase (AK) levels; and intracellular adenosine triphosphate (ATP) content.
4. Qualify the MDA-MB-231 TNBC spheroid model by evaluating its reactivity to treatment.

CHAPTER TWO

2.0 LITERATURE REVIEW

2.1 HALLMARKS OF CANCER

2.1.1 Maintaining proliferative signalling

The most fundamental trait of cancer cells involves their ability to sustain chronic proliferation. This refers to the ability of cancer cells to activate signalling pathways that promote cell growth and division. Normally, these pathways are tightly regulated, but in cancer cells, they are constantly activated, allowing the cells to continue to divide and proliferate even in the absence of normal growth signals. This can be the result of mutations in genes that encode proteins involved in these signalling pathways, leading to the activation of downstream signalling molecules that promote cell growth (Hanahan, 2022, Hanahan and Weinberg, 2017). Growth factor receptor tyrosine kinases (RTKs); the epidermal growth factor receptor (EGFR); small GTPases (Ras); serine/threonine kinases (Raf and Akt); cytoplasmic tyrosine kinases (Src and Abl); lipid kinases (phosphoinositide 3-kinases, PI3Ks); and nuclear receptors (the oestrogen receptor, ER) are examples of proteins involved in signalling pathways that are frequently activated in many physiological responses. Wnt, Hedgehog (Hh), Hippo, and Notch are examples of components of developmental signalling pathways that may also be impacted (Sever and Brugge, 2015).

2.1.2 Eluding growth suppressors

In general, cancer cells are not easily affected by signals from their neighbours that stop them from growing. Cells have internal mechanisms that limit cell growth and division in order to strictly regulate cell division. Tumour suppressor genes are proteins that control these processes. These genes use information from the cell to check if it is prepared to

divide; if not, they will stop the cell from dividing (for instance, if the DNA is damaged) (Weinberg and Hanahan, 2000). In cases of severe abnormalities in the cell, these tumour suppressor proteins are modified in cancer to lose their ability to stop cell proliferation effectively. Normal cells stop dividing when they occupy available space and come into contact with other cells. This mechanism, called contact inhibition, helps prevent cells from proliferating excessively. Because cancer cells lack contact inhibition, they proliferate and divide independently of their environment (Weinberg and Hanahan, 2000, McClatchey and Yap, 2012) .

2.1.3 Enable replicative immortality

Non-cancerous cells are restricted to a few cycles of replication. Telomeres are specialised nucleic acid-protein complexes that preserve the genomic integrity of healthy cells (Jafri et al., 2016). Genomic instability results from the telomeres being shortened by successive cell cycle divisions (Harley et al., 1990). Two defence mechanisms are in place to stop healthy cells from replicating indefinitely. Senescence, the triggering of permanent cell cycle arrest and tissue remodelling, eliminates cells with broken telomeres (Muñoz-Espín and Serrano, 2014). Cells undergo a telomeric crisis phase, marked by cytogenic abnormalities and cell death when severe telomere damage takes place. Most cancer cells can evade senescence and telomeric crisis because the telomerase enzyme lengthens telomeres. This ultimately increases the cancer cells' capacity for unrestricted replication and survival (Jafri et al., 2016).

2.1.4 Resisting cell death

Resisting programmed cell death is one of the basic mechanisms by which tumours are able to establish themselves. While apoptosis was once thought to be the principal type of programmed cell death, it is now widely accepted that there are many different types of programmed mechanisms through which cell death can occur (Zhu et al., 2022). In 2018, the Nomenclature Committee on Cell Death proposed 13 different types of programmed cell death, including the traditional forms of autonomous death, such as

apoptosis, necroptosis, autosis, ferroptosis, and netosis, as well as the newly developed notion of non-cell-autonomous death such as entosis, which is mediated by the creation of cell-in-cell structures (CICs). New mechanisms of cellular death, including cuproptosis, are always being discovered. Almost all types of cell death have been, in some way, connected to human cancers due to the critical role that preventing cell death plays in the formation and spread of tumours (Zhu et al., 2022).

2.1.5 Induce/access vasculature

The hallmark of 'inducing angiogenesis' or 'access to vasculature' refers to the capability of cancer cells to promote the formation of new blood vessels (angiogenesis) to sustain their growth and metastasis. Angiogenesis is the process by which new blood vessels form from pre-existing ones (Hanahan and Weinberg, 2011). In cancer, tumours require sufficient blood supply to provide oxygen and nutrients and to remove waste products. Cancer cells can secrete pro-angiogenic factors, such as vascular endothelial growth factor (VEGF), fibroblast growth factor (FGF), and angiopoietin, which stimulate the growth of new blood vessels from nearby vessels (Carmeliet and Jain, 2011). The tumour microenvironment (TME) plays a crucial role in angiogenesis. Cancer cells, along with stromal cells, immune cells, and extracellular matrix (ECM) components, create a pro-angiogenic environment within the tumour. This environment is characterised by hypoxia (low oxygen levels), inflammation, and the release of growth factors and cytokines that promote angiogenesis (Carmeliet and Jain, 2011). Angiogenesis supports primary tumour growth and facilitates the metastatic spread of cancer cells to distant organs. Newly formed blood vessels provide a route for cancer cells to enter the bloodstream and disseminate to other parts of the body, where they can establish secondary tumours (Folkman, 2002).

2.1.6 Active invasion and metastasis

Active invasion and metastasis refer to the ability of cancer cells to invade surrounding tissues and spread to distant organs, leading to the formation of secondary tumours

(Hanahan and Weinberg, 2011). Cancer cells acquire the ability to invade surrounding tissues by breaking down the ECM and basement membrane barriers through various mechanisms, including the secretion of proteolytic enzymes such as matrix metalloproteinases (MMPs). This allows cancer cells to migrate into adjacent tissues and establish local invasion (Valastyan and Weinberg, 2011). Metastasis is the process by which cancer cells spread from the primary tumour to distant sites in the body. To metastasise, cancer cells must intravasate into nearby blood or lymphatic vessels, survive in the circulation, extravasate into distant tissues, and establish secondary tumours at metastatic sites (Sznurkowska and Aceto, 2022). Metastasis involves intricate interactions between cancer cells and the host microenvironment, including interactions with stromal cells, immune cells, and the ECM (Lambert et al., 2017).

2.2 BREAST CANCER

Breast cancer is a type of cancer that originates in the breast and frequently spreads to distant organs such as the bone, liver, lung, and brain. Numerous factors can increase the likelihood of developing breast cancer, including gender, ageing, oestrogen, family history, gene mutations, and unhealthy lifestyle choices. A positive prognosis and high survival rate can result from early diagnosis of the illness (Sun et al., 2017). Mammography is a popular screening method for finding breast cancer and has been shown to lower mortality significantly. Over the past ten years, additional screening techniques, such as Magnetic Resonance Imaging (MRI), which is more sensitive than mammography, have also been used and researched (Sun et al., 2017). The World Health Organization (WHO) states that the establishment of breast cancer policies continues to improve breast cancer outcomes and survival rates through early detection. To treat breast cancer, various contemporary medicines are prescribed. The medical treatment of breast cancer with anti-oestrogens like raloxifene or tamoxifen may prevent breast cancer in people who are more likely to get it (Akram et al., 2017). A further preventative strategy in cases where a woman's risk of acquiring cancer is higher is having both breasts

surgically removed. Different management techniques, such as targeted therapy, hormonal therapy, radiation therapy, surgery, and chemotherapy, are applied to patients who have been diagnosed with breast tumours. Management strategies for people with distant metastases are typically intended to improve life expectancy and survival rates (Akram et al., 2017).

2.2.1 Breast cancer screening

Breast cancer screening methods aim to detect breast cancer at an early stage when it is most treatable (Coleman, 2017). The main screening methods for breast cancer include:

1. **Mammography**: This is the most common screening tool for breast cancer. It involves taking X-ray images of the breast tissue. Screening mammograms are typically recommended for women aged 40 and older, although guidelines vary by country and organisation. Diagnostic mammograms may be performed if any abnormalities are found during screening or if a woman has symptoms (Reeves and Kaufman, 2020).
2. **Clinical breast examination (CBE)**: This involves a healthcare provider manually examining the breasts for any lumps or abnormalities. While CBE was once a standard part of breast cancer screening, its role has become less clear in recent years, with some organisations no longer recommending it as a routine screening tool (Huang et al., 2022).
3. **Breast self-examination (BSE)**: BSE involves women examining their own breasts regularly to detect any changes or abnormalities. However, the effectiveness of BSE as a screening tool is debated, and it is no longer recommended as a routine screening method by most healthcare organisations. Instead, women are encouraged to be aware of their breasts' normal appearance and report any changes to their healthcare provider (Dewi et al., 2022).
4. **Breast MRI**: Magnetic resonance imaging (MRI) can serve as a screening tool for women at elevated risk of breast cancer, including those with a strong family history of the disease or those carrying specific genetic mutations (e.g., BReast

CAncer gene 1 (BRCA1) or BReast CAncer gene 2 (BRCA2)). Breast MRI is more sensitive than mammography but is also more expensive and may result in more false-positive findings (Gao et al., 2021b).

5. **Breast ultrasound**: This uses sound waves to produce images of the breast tissue. It may serve as a supplementary screening tool in women with dense breast tissue or to evaluate further abnormalities found on mammograms or clinical breast examinations (Boca et al., 2021).
6. **Three-dimensional mammography (tomosynthesis)**: Also known as digital breast tomosynthesis, this advanced form of mammography provides 3D images of the breast tissue, which can improve cancer detection rates and reduce false-positive results compared to traditional mammography (Gao et al., 2021a).

2.2.2 Risk factors of breast cancer

Breast cancer risk factors can be divided into two main categories:

1. **Non-modifiable risk factors**: These are factors that you cannot change.
   a. **Gender**: Being female is the primary risk factor for breast cancer (Sun et al., 2017).
   b. **Age**: The risk of breast cancer increases with age, with most cases occurring in women over 50 years (Lima et al., 2021)
   c. **Family history**: Family history is linked to about 25% of incidents of breast cancer. Having a first-degree relative (parent, sibling, or child) with breast cancer increases the risk of developing breast cancer. Mutations in genes linked to breast cancer, including BRCA1 and BRCA2, are partly responsible for the inherited predisposition to breast cancer (Sun et al., 2017).
   d. **Personal history**: An individual who had breast cancer before has a higher risk of developing it in the other breast or a different part of the same breast (Sierra et al., 2021).

2. **Modifiable risk factors**: These are factors that can potentially be changed or controlled. These are listed below:

a. **Lifestyle factors**: Certain lifestyle choices can influence the risk, such as excessive alcohol consumption, lack of physical activity, being overweight or obese (especially after menopause), and smoking (Cohen et al., 2023).
b. **Hormone replacement therapy (HRT)**: Long-term use of hormone replacement therapy after menopause can increase the risk of breast cancer (Tan and Dayu, 2022).
c. **Reproductive factors**: Early onset of menstruation (before age 12) or late menopause (after age 55), having a first child after age 30, or never having children can affect the risk. A one-year postponement of menopause results in a 3% rise in the risk of breast cancer. The risk of breast cancer drops by 5% and 10% for every year that menarche is delayed or for every extra birth, respectively (Sun et al., 2017).
d. **Radiation exposure**: Previous radiation treatment to the chest area, particularly during adolescence, increases the risk of breast cancer later in life (Moskowitz et al., 2021).
e. **Dietary factors**: While research is ongoing, some studies suggest that a diet high in saturated fat and low in fruits and vegetables may increase the risk of breast cancer. The consumption of more vegetables and fibre is linked to a decrease in serum oestrogen levels; a reduction in total and plasma oestradiol levels; and an increase in oestrogen linked to globulin, which affects the bioavailability of oestradiol. At its onset, breast cancer is linked to these oestrogen levels (Guerrero et al., 2017).

2.2.3 Molecular genetics of breast cancer

There are many genes that have been linked to breast cancer. Oncogene and anti-oncogene mutations and abnormal amplification play important roles in the development and spread of tumours (Sun et al., 2017).

2.2.3.1 BRCA 1/2

Two widely recognised anti-oncogenes for the risk of breast cancer are breast cancer-associated genes 1 and 2 (BRCA1 and BRCA2). The BRCA genes are found on chromosomes 13q12 and 17q21, respectively. Breast and other cancers are more likely to develop when one of the BRCA1 or BRCA2 genes is mutated. Large deletions and rearrangements in BRCA1 or BRCA2 can also affect how the genes operate, causing an analogous clinical condition to that found in carriers of these gene abnormalities. Although some patients with the same clinical picture are found to be negative for both BRCA1 and BRCA2 mutations, the clinical syndrome seen in BRCA mutation carriers is known as the hereditary breast/ovarian cancer (HBOC) syndrome (Shiovitz and Korde, 2015).

2.2.3.2 Human Epidermal Growth factor receptor 2 (HER-2)

Growth factor receptors, such as the human epidermal growth factor receptor 2 (HER-2) gene, activate intracellular signalling pathways in response to growth factors, which are extracellular messengers. When these intracellular processes are disrupted, whether by HER-2 mutations or overexpression, they can result in cancer formation. These intracellular processes promote controlled cell proliferation and embryonic development (Galogre et al., 2023). Numerous cancers, including breast, colorectal, bladder, gastric, oesophageal, endometrial, and ovarian cancers, have been found to have HER-2 overexpression and mutations. Treatment and results related to their treatment can be affected by the existence of HER-2 dysregulation or overexpression caused by somatic mutations in certain malignancies (Galogre et al., 2023, Iqbal and Iqbal, 2014). After it was discovered that HER-2 can induce mammary carcinogenesis *in vitro* and *in vivo*, the majority of HER-2 studies have been conducted on breast cancer. About 15 - 30% of breast cancers have HER-2 gene amplification or overexpression (Iqbal and Iqbal, 2014). HER-2 overexpression has prognostic significance in breast cancer regardless of the type of treatment given (or if there is no treatment), as it indicates a more aggressive and deadly form of cancer (Galogre et al., 2023).

2.2.3.3 Epidermal Growth Factor Receptor (EGFR)

A tyrosine kinase, known as the EGFR, has a role in the growth, division, and mitosis of cells as well as the development of cancer. Additionally, it has a significant impact on the emergence of drug resistance (Sabbah et al., 2020). The EGFR is a trans-membrane glycoprotein that has a cytoplasmic tyrosine kinase domain and an extracellular ligand-binding domain. Numerous downstream signalling pathways, including RAS/RAF/MEK, STAT, and PI3K/AKT/mTOR, are initiated when the intracellular tyrosine kinase domain of receptors is activated and auto-phosphorylated. Following the occurrence of a series of different events in the cytoplasm, cells proliferate, survive, and experience an inhibition of apoptosis (Ayati et al., 2020). More than 30% of cases of inflammatory breast cancer (IBC), an extremely aggressive subtype of breast cancer, exhibit overexpression of EGFR. Patients with IBC who test positive for EGFR have a worse prognosis than those who test negative for EGFR. EGFR overexpression is present in more than half of TNBC instances, which are distinguished by the absence of ER, PR, and HER-2 amplification (Sun et al., 2017).

2.3 TRIPLE-NEGATIVE BREAST CANCER

TNBC is a form of breast cancer in which the HER-2, PR, and ER are all not expressed (Yin et al., 2020). Due to its lack of molecular targets, chemotherapy is the sole known treatment option for this physiologically and clinically diverse disease. This has long been regarded as a large unmet need due to this cancer's aggressive behaviour and poor prognosis (Bianchini et al., 2022). TNBC is characterised by shorter overall survival and an early peak of distant recurrences at three years following diagnosis. Most deaths occur within the first five years of a diagnosis. With this breast cancer subtype, late tumour recurrences are uncommon, and recurrences typically do not manifest themselves after eight years (Collignon et al., 2016). TNBC patients mostly show greater resistance to treatment than breast cancers that are hormone receptor (HR) positive. Patients with TNBC only live a year once their malignancies spread to their visceral organs. Thus, a

diagnosis of metastatic TNBC always comes with death as a high and ultimate possibility for the patient (Figure 2.1) (Garlapati et al., 2019).

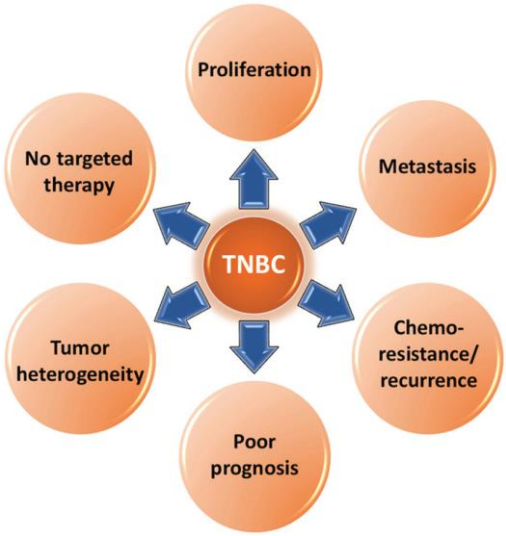

Figure 2.1: Variety of critical aspects attributed to triple-negative breast cancer aggressiveness (Garlapati et al., 2019).

2.3.1 TNBC treatment

Although it is widely acknowledged that early-stage TNBC is sensitive to chemotherapy, the ideal course of treatment is still unknown. The standard treatment for a locally advanced or inoperable TNBC is neoadjuvant chemotherapy. The capacity to anticipate survival based on the existence or absence of a pathological complete response (pCR) at the time of surgery and to customise adjuvant therapy is a significant benefit of this technique. Patients with TNBC are more likely to achieve a pCR with neoadjuvant chemotherapy than patients with luminal subtypes (Bergin and Loi, 2019). Anthracyclines (such as the DNA intercalating agent and topoisomerase II inhibitor doxorubicin), alkylating drugs (such as cyclophosphamide), an anti-microtubule agent taxane, and anti-metabolite fluorouracil (5-FU) are examples of common chemotherapies. Neoadjuvant chemotherapy is currently the standard of care (SOC) for newly diagnosed early TNBC, which is followed by surgery. There is no typical chemotherapy regimen for people with relapsed/refractory TNBC. Treatment responses are frequently transient, swiftly followed

by relapse, and visceral and brain metastases are frequent (Won and Spruck, 2020). Relapsed and metastatic TNBCs are frequently more aggressive, displaying considerable resistance to chemotherapy (Bai et al., 2021). Antimetabolites capecitabine and gemcitabine, non-taxane microtubule inhibitor eribulin, and DNA cross-linker platinums are among the treatments that are available for patients with advanced TNBC (Won and Spruck, 2020). pCR rates for anthracyclines alone ranged from 14 to 47%, whereas pCR rates for sequential anthracycline plus taxane regimens ranged from 17 to 39%. For TNBC treated with neoadjuvant anthracyclines, cyclophosphamide, and taxanes, GeparTrio demonstrated pCR rates up to 57% (Bergin and Loi, 2019).

2.3.2 Doxorubicin

Doxorubicin (DOX) is an antibiotic generated from the antibiotic bacteria *Streptomyces peucetius*. As a chemotherapeutic agent, it has been widely used since the 1960s (Johnson-Arbor and Dubey, 2017). Doxorubicin belongs to the anthracycline class of chemotherapy drugs, along with daunorubicin, idarubicin, and epirubicin. It is a medication frequently used to treat solid tumours in both adult and paediatric patients. Breast, ovarian, bladder, thyroid, soft tissue and bone sarcomas can all be treated with doxorubicin. Additionally, Hodgkin lymphoma, acute myeloblastic leukaemia, acute lymphoblastic leukaemia, and small-cell lung cancers are all treated with it (Johnson-Arbor and Dubey, 2017). To have its desired effects, DOX must intercalate into DNA and inhibit topoisomerases I and II. This results in DNA damage, generation of reactive oxygen species (ROS), activation of caspases, and finally, apoptosis (Figure 2.2). Sadly, DOX can also lead to cardiotoxicity (Franco et al., 2018). Resistance mechanisms unique to topoisomerase II inhibitors have been determined to include increased efflux and changes to topoisomerase II expression (Lovitt et al., 2018). Many factors linked to acquired or *de novo* mechanisms might lead to resistance to treatments. While *de novo* resistance is primarily related to a tumour's properties that predate anti-cancer drug use, acquired resistance mechanisms develop in response to exposure to the treatments.

Environmental factors, such as cancer cells adhering to stromal components, including the ECM, can mediate *de novo* resistance (Lovitt et al., 2018).

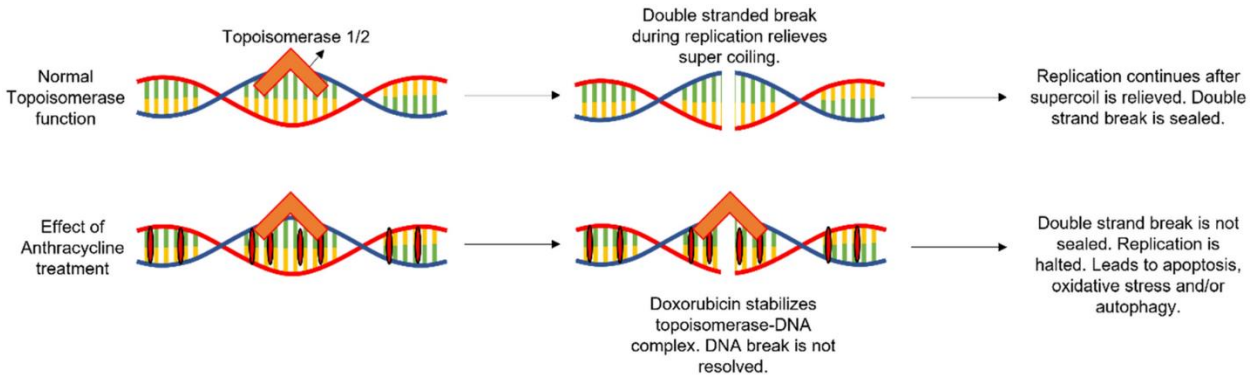

Figure 2.2: The mechanism of action of anthracycline doxorubicin (Mandapati and Lukong, 2023). Figure reproduced under a Creative Commons Attribution 4.0 International License http://creativecommons.org/licenses/by/4.0/).

2.3.3 Heterogeneity in TNBC

Understanding the heterogeneity of TNBC is a milestone in TNBC treatment. In landmark studies based on genomic and transcriptomic data, Jiang et al., in 2019, proposed four molecular subtypes of breast cancer: basal-like (BL); mesenchymal-like (MES); immunomodulatory (IM); and luminal androgen receptor (LAR) (Bai et al., 2021). Most BL tumours are triple-negative, resulting in the misunderstanding that both terms are interchangeable. Although 70 - 80% of TNBC are BL, roughly 70% of basal-like breast cancers are triple-negative. The BL and immune-suppressed (BLIS) subtypes are characterised by the activation of DNA repair and downregulation of immune response genes, while the androgen receptor-associated (LAR) subtype exhibits androgen receptor signalling. The MES subtype is enriched in breast cancer stem cell pathways (Lehmann et al., 2015).

The MES is enriched for genes involved in cell motility and epithelial-mesenchymal transition (EMT) and is associated with a greater signature score for angiogenesis (Marra et al., 2020). The MES subtype is susceptible to developing drug resistance and possesses

tissue features resembling sarcomas or squamous epithelial cells. Therefore, mTOR inhibitors or medications that target the epithelial-mesenchymal transition may be used to treat MES-subtype patients (Yin et al., 2020). The definition of the LAR sub-type as a variation of TNBC involves numerous morphological, molecular, and genetic characteristics, in addition to the existence of an indicator of AR-positive expression (Vtorushin et al., 2022). Tumours are classified as IM type, BLIA type, or basal-enriched with high immune response and low M2-like macrophages, which are included in the IM subtype. The prognosis of the IM subtype is better than that of the other TNBC subtypes. Additionally, the meta-analysis shows that a high number of tumours infiltrating lymphocytes (TILs) is associated with a good prognosis in TNBC (Polk et al., 2018). A TNBC subtype with no basal markers has recently been discovered, which is the intrinsic claudin-low molecular subgroup. This subgroup includes cancers that have increased levels of markers for stem cells and the EMT (Nedeljković and Damjanović, 2019, Marra et al., 2020).

2.4 DRUG RESISTANCE IN TNBC

Drug resistance to chemotherapeutic agents is a significant challenge in the effective treatment of cancer, particularly in a metastatic situation, where it is responsible for 90% of unsuccessful therapy (Nedeljković and Damjanović, 2019). Drug resistance can be caused by a variety of mechanisms, one of the most well-known being transporter-mediated drug efflux (Guestini et al., 2019). ATP-binding cassette (ABC) transporters (Figure 2.3) cause ATP-dependent outflow of various substances across the cellular membranes, including various antineoplastic drugs. Multidrug-resistant protein-1 (ABCC1/MRP1) or P-glycoprotein (P-gp), breast cancer-resistant protein (ABCG2/BCRP), and multidrug-resistant protein 8 (ABCC11/MRP8) all have considerably increased expression or overexpression in TNBC, compared to other subtypes of breast cancer (Marra et al., 2020). The discovery that neoadjuvant chemotherapy elevates ABCC1 protein expression in TNBC supports the function of ABCC1 in TNBC drug resistance. Furthermore, the stimulation of the Hh pathway in TNBC cells leads to the development

of drug resistance as a result of the upregulation of ABC transporters. ABCG2 is closely associated with drug resistance of stem cells in TNBC. The downregulation of ABCG2 via suppression of the growth hormone receptor results in chemosensitivity of TNBC cells, confirming its relevance in TNBC resistance (Nedeljković and Damjanović, 2019).

Drug resistance in TNBC could also result from cancer stem cells (CSCs) (Figure 2.3), a tumour cell subgroup that can self-renew after chemotherapy, resulting in tumour re-growth (He et al., 2021). Despite the fact that CSCs have been found in all subtypes of breast cancer, TNBC was found to be fundamentally rich in CSCs. Furthermore, after neoadjuvant chemotherapy, it was found that there was an increase in drug-resistant CSCs in residual tumours (Nedeljković and Damjanović, 2019). CSC-associated drug resistance could be a result of a number of variables, such as their low growth rate and overexpression of ABC transporters. Targeting CSC surface antigens and signalling pathways important for CSC self-renewal are among the therapeutic strategies being evaluated to overcome CSC drug resistance (Marra et al., 2020).

Another known mechanism that promotes tumour development, survival and drug resistance is hypoxia (Figure 2.3). Hypoxia modifies the TME, impairing the absorption and/or activity of several cytotoxic drugs and conferring drug resistance. Hypoxia also brings about the phenotype of breast CSCs and promotes immunosuppression (Marra et al., 2020). TNBC is typically associated with high levels of hypoxia and frequently exhibits hypoxia-related morphological characteristics, for example, the existence of fibrotic and necrotic regions (Nedeljković and Damjanović, 2019). Hypoxia may be targeted with hypoxia-activated pro-drugs functioning as cytotoxins or by the suppression of molecular targets important for hypoxia processes, such as hypoxia-inducible factor inhibitors (Marra et al., 2020).

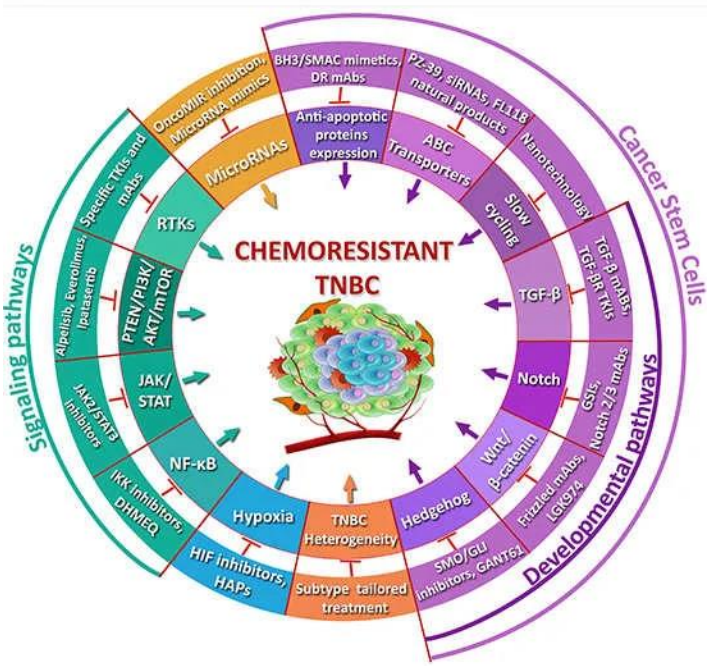

Figure 2.3: Contributors of chemo-resistance in triple-negative breast cancer (Nedeljković and Damjanović, 2019). Figure is reproduced under the terms and conditions of the Creative Commons Attribution (CC BY) license (http://creativecommons.org/licenses/by/4.0/**).**

2.5 CELL-BASED MODELS TO STUDY DRUG RESISTANCE

The 2D cell-based models are simple, practical, cost-effective, and widely employed. However, in contrast to *in vivo* conditions, 2D culture models of tumours (i) lack the mechanical and natural structure of tumours; (ii) lack heterogeneous tumour populations; (iii) lack cell-cell and cell-stroma interactions; (iv) have limitless access to oxygen, nutrients, metabolites, and signal molecules (Figure 2.4 A); (v) poorly represent cell proliferation, differentiation, cell hierarchy, gene and protein expression, response to perturbations, stimuli, and drugs, migration, and invasion; and (vi) lack interactions between cells and the ECM (Pozzi et al., 2021). Additionally, 2D cell-based models continue to be overly simplistic models that do not replicate how tissue is organised *in vivo*, especially the TME. The ECM, which is a network of macromolecules (primarily proteoglycans, collagen, laminin, elastin, and enzymes), water, cytokines, and growth

factors, is a non-cellular component of the TME. Immune cells such as T cells, B cells, natural killer cells, macrophages, neutrophils, and dendritic cells are also included in the ECM. The tumour host tissue, the type of malignancy, and the patient all affect the content and ratio of each TME component. When researching cancer *in vitro*, it is important to keep in mind that the TME has been demonstrated to play a major role in carcinogenesis, cancer development, and cancer resistance (Jubelin et al., 2022). Three-dimensional cell-based models have characteristic features closely resembling the *in vivo* microenvironment, such as significant cell-cell and cell-ECM signalling. Unlike 2D cell-based models, 3D models may exhibit biochemical and morphological characteristics that are similar to their respective tissues *in vivo* (Ryan et al., 2016).

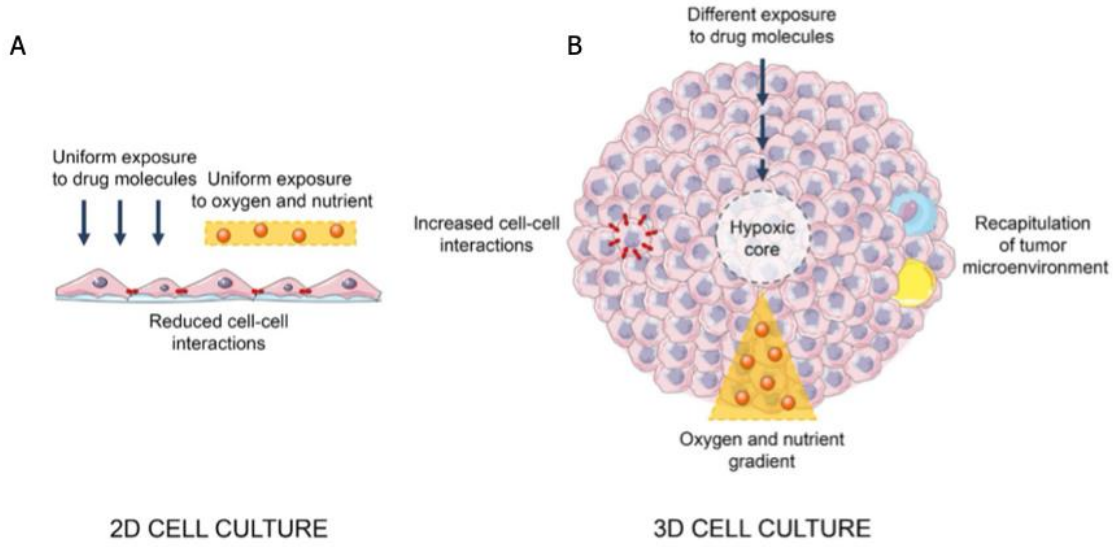

Figure 2.4: Key differences between two-dimensional and three-dimensional cultures (Fontana et al., 2020).

2.5.1 Role of architectural makeup in drug resistance

Mammalian cell culture is a valuable tool for cancer research to study drug efficacy and for drug screening. To date, most cell-based assays rely on standard 2D monolayer cells grown on flat and inflexible substrates. Two-dimensional cell cultures, however, fail to

fully take into consideration the normal biological environment of cells because, in the *in vivo* setting, most of the cells are surrounded by ECM, with other cells in a 3D manner. Thus, *in vitro* responses from 2D cell culture assays can occasionally be misleading and non-predictive (Edmondson et al., 2014, Antoni et al., 2015). As a result of these limitations, 3D cell-based models have emerged as a promising approach for drug screening due to their architectural and physiological similarities to the *in vivo* environment. When cells are cultured using 3D culture methods, they can bring about spheroid formation, depending on the method used, within a matrix. These spheroids' cell-cell and cell-ECM interactions (Figure 2.4 B) are more similar to the normal environment present in a living system so that the cell structure better mimics its normal form in the body. Furthermore, cells in 3D culture go through several stages, including proliferative, quiescent, hypoxic, and necrotic (Figure 2.5). These stages are similar to those in a solid tumour (Chaicharoenaudomrung et al., 2019). Solid tumours are characterised by an antagonistic environment with oxygen, nutrition, and metabolite gradients; they also have complex 3D architecture, high interstitial pressure, and heterogeneous cell populations (such as quiescent and proliferative). By modifying intratumor distribution, cellular absorption, and drug stability, these factors work together to reduce chemotherapeutic efficacy (Hall et al., 2004).

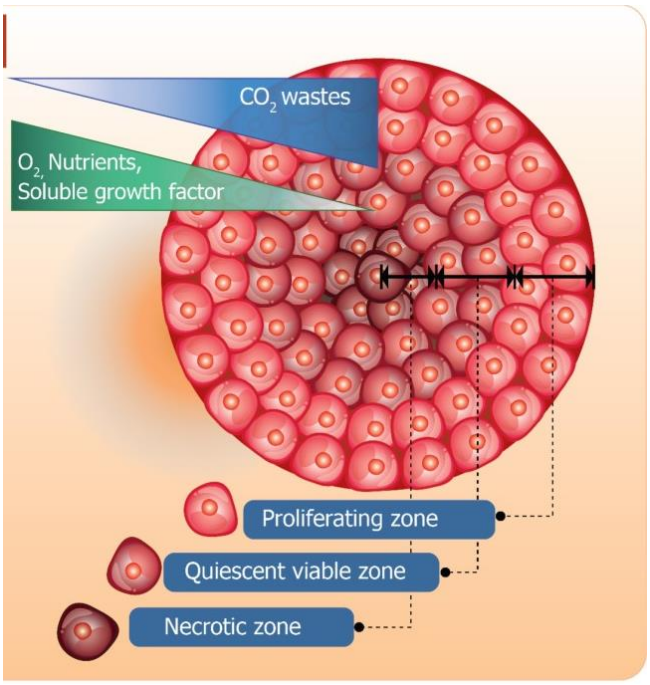

Figure 2.5: The structure of a three-dimensional spheroid with cells distributed in multiple layers, creating zones based on access to oxygen, nutrition, and ability to remove CO_2 waste build-up. The zones are the necrotic zone (innermost), the quiescent viable cell zone (middle), and the proliferating zone (outermost) (Chaicharoenaudomrung et al., 2019). Figure distributed in accordance with the Creative Commons Attribution Non-Commercial (CC BY-NC 4.0) license.

2.5.2 Role of oxygen and nutrient distribution in drug resistance

When a cell suspension is grown in a petri dish, it forms a flat monolayer. These cells have access to equal amounts of oxygen and nutrients (Figure 2.4 A). This accessibility does not reflect what occurs in the TME, where the mass and form of the tumour affect the gradients of nutrients and oxygen (Brancato et al., 2020). However, in 3D spheroids, proliferating cells can be detected on the spheroids' outer layer because they receive enough oxygen and nutrients from the culture medium. However, cells at the centre of the spheroid are usually hypoxic due to oxygen and nutrient deprivation (Figure 2.4 B). The heterogeneity of cells in a cell population is very important to *in vivo* tissues and tumours (Chaicharoenaudomrung et al., 2019). Tumour cells frequently exhibit reduced

sensitivity to drugs in 3D compared to their 2D counterparts. This is a result of multiple factors, but it is mostly regulated by hypoxia, which occurs in the oxygen-deficient areas of the tumour. Therefore, hypoxia is a compelling therapeutic target, given that it plays a key role in tumour development and drug resistance (Kapałczyńska et al., 2018).

Table 2.1: Comparison of two-dimensional and three-dimensional cell culture methods: *adapted from* (Kapałczyńska et al., 2018).

Type of culture	**2D**	**3D**
Time of culture formation	Within minutes to a few hours	From a few hours to a few days
Culture quality	High performance, reproducibility, long-term culture, easy to interpret, simplicity of culture	Worse performance and reproducibility, difficult to interpret, cultures more difficult to produce
In vivo imitation	Does not mimic the natural structure of the tissue or tumour mass	*In vivo* tissues and organs are in 3D form
Cells interactions	Deprived of cell-cell and cell-ECM interactions; no *in vivo*-like microenvironment and no 'niches'	Proper interactions of cell-cell and cell-ECM; environmental 'niches' are created
Characteristics of cells	Changed morphology and way of division; loss of diverse phenotype and polarity	Preserved morphology and way of divisions, diverse phenotype and polarity
Access to essential compounds	limitless access to oxygen, nutrients, metabolites and signalling molecules (in contrast to *in vivo*)	Variable access to oxygen, nutrients, metabolites and signalling molecules (same as *in vivo*)
Molecular mechanisms	Changes in gene expression, mRNA splicing, topology and biochemistry of cells	Expression of genes, splicing, topology and biochemistry of cells as *in vivo*

2.5.3 ECM composition in drug resistance

It is evident that 2D cultures do not accurately represent the complicated TME. The growing understanding of the cell-ECM interactions is one of the most significant influences on the limited physiological value of 2D cell culture. ECM constituents were initially thought to provide mostly structural support, but they are now known to have a tissue-specific effect on most aspects of cellular activity (Langhans, 2018). ECM molecules include matrix proteins, glycoproteins, glycosaminoglycans, proteoglycans and other released proteins. These components are crucial in regulating cell proliferation, adhesion, differentiation, migration, and survival. Additionally, the structure of the ECM can influence how a cell responds to drugs by changing the mechanism of action, enhancing drug efficacy or amplifying a cell's affinity for drug resistance (Jensen and Teng, 2020).

2.6 3D IN VITRO MODELS

The technology used to construct 3D cancer models also classifies them as scaffold-free or scaffold-based systems (Brancato et al., 2020).

2.6.1 Scaffold-free systems

Using a single-cell suspension, spheroid cell aggregates, tissue strands, or cell sheets as building blocks, the scaffold-free method is a 'bottom-up' strategy. The method relies on the building blocks' innate capacity to join and form larger structures (Alghuwainem et al., 2019). In scaffold-free techniques, various factors, such as low-adhesion substrates, gravitational forces, and magnetic actions, play a role in the formation of cellular aggregates and spheroids. Throughout this process, ECM is generated as spheroid cells continuously deposit proteins (Pinto et al., 2020). It involves the culturing of cells into aggregates or spheroids using various methods, such as the hanging drop method, rotating micro-gravity bioreactors, and ultra-low attachment plates, amongst others (Thoma et al., 2014).

2.6.1.1 Hanging drop method

This method is based on growing cells in a suspended drop of medium, which enables the cells to group together and create 3D models at the bottom of the droplet (Badea et al., 2022). Using this technique, phosphate-buffered saline (PBS) is added to a petri dish lid and around 25 µl of the cell suspension to prevent the cellular solution from dehydrating. After that, the lid is turned upside down, but the droplets stay suspended because of surface tension. The cells in the droplets aggregate naturally under gravity, resulting in the formation of a single spheroid. Large-scale spheroidal synthesis and simple size control are made possible by this technology. However, because of its multistep method and potential for cell harm in the event of medium evaporation, it requires continual monitoring of the culture medium, which is labour-intensive labour (Pinto et al., 2020).

2.6.1.2 Micro-gravity bioreactors

Three-dimensional spheroids can grow in bioreactors, which are instruments that monitor and regulate many environmental parameters, including pH, temperature, shear stress, pressure, nutrient delivery, and waste removal. Bioreactors decrease the concentration boundary layer often found in static cultures by ensuring that oxygen and nutrients are evenly mixed throughout the medium (Smit et al., 2020). The ClinoStar™ system will be used in this study to grow 3D spheroids. This suspension culture system permits the development of 3D spheroids under low physiological fluid shear conditions (Radtke and Herbst-Kralovetz, 2012).

2.6.1.3 Ultra-low attachment plates

A substrate is applied to the plate surfaces to inhibit cell attachment and encourage cell aggregation and spheroid formation. In addition to having minimal adhesion, the wells on these plates have a specified shape, a round bottom, and are V-shaped or conical, which makes it possible to create a single spheroid (Pinto et al., 2020). Typically, agar/agarose or poly (2-hydroxyethyl methacrylate) are the primary substrates used to coat the plate, and 50 µl of solution at concentrations of 15 mg/ml and 5 mg/ml is added

to each well of 96-well plates. This method allows for the simultaneous generation of many spheroids on a single plate, which improves experimental reproducibility and makes it possible to track the development and growth of spheroids. One drawback of ultra-low attachment plates is that certain tumour cell lines are unable to produce tightly packed spheroids (Pinto et al., 2020).

2.6.1.4 Spinner flasks

Culturing cells in a container with an agitator is one of the methods for obtaining spheroids, as cells cannot attach to the substrate/container under these conditions, so they start to aggregate and self-assemble. It is the most straightforward way to make spheroids on a large scale (Ryu et al., 2019). This technique has some drawbacks, such as culture lifetime, spheroid size variance, and mechanical injury to cells, but it largely depends on the mechanism of agitation.

2.6.1.5 Magnetic levitation

One new method for creating spheroids is magnetic cell levitation. To create spheroids, cells that have been preloaded with magnetic nanoparticles are floated towards the air/liquid interface in a low adhesion plate with the help of an externally produced magnetic field. This process facilitates cell-cell aggregation and the production of spheroids. Magnetic levitation has been applied to tissue engineering, multicellular mesenchymal stem cell spheroids, and the generation of spheroids from cells of different tissues (Langhans, 2018). The *in vivo* protein expression of human glioblastoma tumour xenografts was closely mimicked by magnetically levitated cells, and this technique is a promising new tool for drug discovery since it was recently used to describe a high-throughput assay for toxicity screening in 3D cell cultures (Langhans, 2018, Timm et al., 2013).

2.6.2 Scaffold-based systems

With the use of scaffold-based culture technologies, cells can gather, multiply, and move on physical support that can range from straightforward mechanical structures to

matrices resembling ECM. Tissue-specific cell differentiation is made possible in 2.5D preparations by the thick layer of ECM proteins on top of which cells are cultured. This technique involves seeding cells on a scaffold (such as collagen), allowing the cells to adhere and colonise (Alghuwainem et al., 2019). These scaffolds provide a physical structure that mimics the ECM found in native tissues, offering support and guidance for cell attachment, proliferation, differentiation, and tissue formation (Abuwatfa et al., 2024). In cancer research, scaffolds promote cancer cell development and can closely resemble the TME, which is shown by fibroblasts' role in depositing ECM (Brancato et al., 2020, Thoma et al., 2014). Scaffolds can be made from various materials, including natural polymers (such as collagen, fibrin, alginate, and chitosan); synthetic polymers (such as poly(lactic-co-glycolic acid) (PLGA), poly(ethylene glycol) (PEG) and polycaprolactone (PCL)); or a combination of natural and synthetic materials. The choice of scaffold material depends on factors such as biocompatibility, mechanical properties, degradation kinetics, and the specific tissue being engineered (Abdelaziz et al., 2023).

2.6.2.1 Matrix encapsulation

To create cellular microcapsules, suspended cells are encased in hydrogel and submerged in a calcium-free solution. Cells group together in these microcapsules to create matrix-encapsulated spheroids (Pinto et al., 2020). Microcapsules typically range in size from 100 to 500 μm, can produce either monotypic or heterotypic spheroids, and facilitate communication between cells and the ECM. Nutrients and metabolic residues are transported in these systems via simple diffusion. As the size of the microcapsule grows, nutrient transport becomes more restricted, which may result in cellular necrosis. Alginate hydrogels have been employed extensively to create microcapsules because of their viscoelastic properties. One significant benefit of this approach is that it produces spheroids with uniform sizes (Pinto et al., 2020).

2.6.2.2 Hydrogels

Hydrogels are 3D networks of hydrophilic polymers, which can be synthetic, natural, or hybrid. They can retain their structural integrity despite absorbing substantial volumes of

water or biological fluids. These networks can be created by intermolecular crosslinking (polymer network) or interfibrillar crosslinking (supramolecular fibrillary hydrogel network) (Abuwatfa et al., 2024, Langhans, 2018). These hydrogels facilitate the passage of O_2, nutrition, waste, and soluble substances while simulating soft, moist conditions that resemble the ECM of natural tissues. Consequently, they have drawn much interest in 3D cell culturing (Park et al., 2021). The capacity of hydrogels to imitate the ECM while permitting soluble components like growth factors and cytokines to pass through the tissue-like gel makes them special. Hydrogels exhibit versatility as well, as they can be prepared in various ways depending on the experiment being conducted, and they can be utilised to generate spheroids. Hydrogels can be manufactured or natural. Natural gels typically comprise natural polymers such as alginate; hyaluronic acid; collagen; Matrigel; gelatin; chitosan; and fibrinogen (Jensen and Teng, 2020).

2.6.2.3 3D bioprinting

Three-dimensional bioprinting is an advanced technology that enables the fabrication of complex 3D structures using living cells, biomaterials, and bioactive molecules. It holds great promise for tissue engineering, regenerative medicine, drug screening, and disease modelling by precisely arranging cells and biomaterials spatially to mimic the architecture and functionality of native tissues and organs (Murphy and Atala, 2014). Compared to other production methods, it allows for more control over pore sizes, pore morphology, and matrix porosity because it includes layering consecutive layers of material to produce 3D models (Loh and Choong, 2013).

Table 2.2: Pros and cons of various methods for creating 3D models.

3D Culture Method	Pros	Cons	References
Ultra-low attachment plates	Comparatively simple Quicker synthesis of spheroids Appropriate for long-term culture Reproducible Inexpensive	Labour intensive Challenge of mass production Inconsistency in size and shape	(Wanigasekara et al., 2023)
Hanging drop	Easy No specific equipment is needed Control of defined spheroid size Consistent spheroid size Co-culture with regulated cellular makeup	Labour extensive Time consuming Unsteady Long-term cultural challenges low speed of operation Ineffective	(Benien and Swami, 2014)
Spinner flask	Easy Mass manufacturing of spheroids Long-term culture	Specific tools needed No individual compartment for each sample Lack of control over spheroid homogeneity (composition and size) Increased shear force in cells	(Benien and Swami, 2014)
ClinoStar™ system	Relatively simple approach Large-scale production Established cultivation	Needs specialized equipment Volume is fixed at 10 ml	(Wrzesinski et al., 2021)

	Comparable medium composition Activates metabolite transport Poor shear forces Identical spheroids Simple medium exchange		
Magnetic levitation	Enhanced effectiveness Simple technique It does not need a specialised medium. Exchange of media is simple.	Makes the 3D structures brown, which restricts its use in several applications. Cells stick to the well bottoms. The behaviour of cells can be impacted.	(van Niekerk et al., 2023, Wanigasekara et al., 2023)
Scaffold-based	Resembles the *in vivo* microenvironment. Easy to handle Compatible with all cell types and well plates.	High costs for large scale production. Inconsistency in size and shape Restricted high-throughput screening.	(Wanigasekara et al., 2023)
Hydrogels	Has flexibility similar to that of tissue. Water-soluble components are easily supplied to the cells.	There is little mechanical resistance.	(Park et al., 2021)
Matrix encapsulation	Favourable conditions for cell survival Regulation of porosity and permeability Simple functionalization Simple alterations to chemicals	Mechanically weak Non-homogeneity of gels Difficulties to sterilize	(Rabanel et al., 2006)

3D bioprinting	Interactions between cells are conceivable. It is possible to replicate 3D tissue architecture. Capable of imitating the chemical composition of a tumour. It is possible to do high throughput screening. Can replicate the intricate relationships that exist between the ECM and the TME in cancer research.	Hard to standardise the procedure. The cell-ECM interactions cannot be replicated. Costly supplies and machinery It is challenging to arrange the cells. There is still room for improvement in the printing resolution optimisation.	(Gómez-Oliva et al., 2021, Kitaeva et al., 2020)

2.7 APPLICATION OF 3D *IN VITRO* MODELS IN DRUG SCREENING

Accurately assessing potential medications for efficacy in pre-clinical models requires recapitulating *in vivo* tissues. For instance, because of their 3D layout, cancer cells exist *in vivo* as a 3D mass with unique metabolic and proliferative gradients (Figure 2.6) (Belfiore et al., 2021). Furthermore, proteins, tumour-associated cells, and soluble substances comprise the ECM surrounding solid tumours. These components all have a role in the biology of the tumour and, as a result, affect how cells respond to treatment (Belfiore et al., 2021). Chemical screens in well-characterised cell monolayers and, primarily for cancer drug discovery, in sizable panels of verified cell lines were the focus of cell-based drug discovery in the past (Langhans, 2018). However, 3D cell culture techniques, which simulate characteristics of the *in situ* microenvironment and are therefore anticipated to produce data with a higher predictive value for clinical outcome, have recently gained prominence in drug research. Authentic 3D cell-based models employing human cells can also avoid the limitations of mice models, which, aside from their high cost and ethical issues, sometimes fail to effectively mimic human diseases or capture therapeutic side effects, such as liver toxicity (Aparicio et al., 2015). For 3D cell-based models to be effective as *in vitro* toxicity screens, they must consider that the response to a wide range of drugs varies, not only with a specific cell line or tumour type but also with its surrounding stroma. This can improve the drug discovery process and help develop new pharmacological approaches (Langhans, 2018). It has been demonstrated that, in contrast to 2D cultures, cellular responses to pharmacological treatments in 3D cultures are more like those that take place *in vivo*. Numerous investigations have revealed that, compared to 2D cultures, cells grown in 3D models exhibit higher resistance to anti-cancer medications (Edmondson et al., 2014). The development of 3D organoid banks of tumour cells that are representative of molecular tumour subtypes, or the combination of 3D cell culture technology with primary patient-derived tumour cells and molecular profiling data, may pave the way for pre-clinical

screening of a customised panel of drug candidates to enhance cancer therapy outcomes and lessen side effects (Ma et al., 2015).

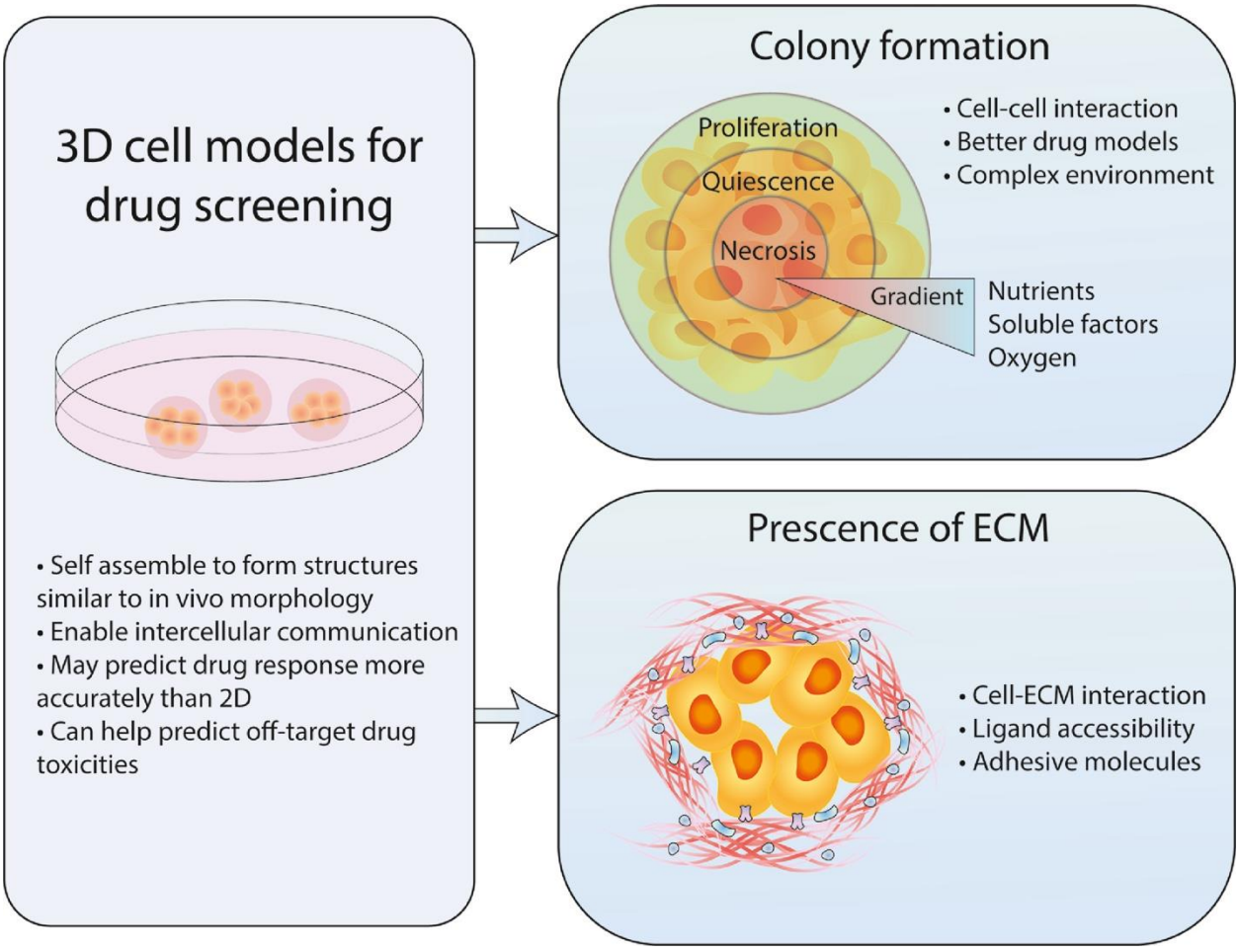

Figure 2.6: Three-dimensional cell models for drug screening. Cells cultured in three-dimension better represent *in vivo* tumours and tissues by recapitulating *in vivo* architecture and the presence of extracellular matrix, which affects drug response (Belfiore et al., 2021).

CHAPTER THREE

3.0 RESEARCH MATERIALS AND METHODOLOGY

3.1 SITE SELECTION:

The execution of the tasks in this research study was conducted at two locations concurrently: the Basic Medical Sciences Department at the University of the Free State in Bloemfontein and Pharmacen™ at North-West University in Potchefstroom.

3.2 MATERIALS

The MDA-MB-231 (HTB-26™) cell line was purchased from the American Tissue Culture Collection (ATCC) through Industrial Analytical (Pty) Ltd, which forms part of LGC standards, the sole supplier of ATCC materials in South Africa. The importation of the cells as biological material in terms of Section 68 of the National Health Act 2003 (Act No. 61 of 2003) was handled by Industrial Analytical (Pty) Ltd. This included the subsequent customs clearance and shipment of materials using cold chain handling to the Basic Medical Sciences Department at the University of the Free State.

The MDA-MB-231 (HTB-26™) cell line, identified as a non-hazardous substance, is classified as a biosafety level 1 product by the ATCC, based on their risk assessment as guided by the current edition of Biosafety in Microbiological and Biomedical Laboratories (BMBL), U.S. Department of Health and Human Services.

Dulbecco's modified eagle medium (DMEM) (with phenol red, Gibco) and foetal bovine serum (FBS) (Gibco) were obtained from Thermo Fisher Scientific (Johannesburg, South Africa). Other consumables also included: L-glutamine (200 mM, Lonza, Whitehead Scientific (Pty) Ltd, Cape Town, South Africa); doxorubicin hydrochloride (Sigma-Aldrich); phosphate-buffered saline (PBS) (1X, HyClone, Separations, Johannesburg, South Africa); Trypsin-Versene (EDTA) (1X, Lonza); a Quick Start™ Bradford Protein assay (Bio-Rad, Lasec SA (Pty) Ltd, Midrand, South Africa); and CellTiter-Glo® Luminescent Cell Viability assay (Promega, Anatech Instruments (Pty) Ltd, Johannesburg, South Africa). Toxilight®

BioAssay (Lonza) and OneTouch® Select™ test strips were used for the various assays. The ClinoReactors™ (CelVivo ApS, Odense, Denmark), purchased from Promolab (Trading as Separation, Johannesburg, South Africa), and the ClinoStar™ system (CelVivo ApS Odense, Denmark), were used for maintenance and to conduct experiments on the spheroids.

3.3 ETHICAL CONSIDERATION

This research protocol was approved by the Environment and Biosafety Research Ethics Committee of the University of the Free State and the Research Ethics Committee (REC) at the North-West University. Ethical clearance number: UFS-ESD2022/0303

3.4 METHODOLOGY

3.4.1 Cell culture and maintenance of 2D MDA-MB-231 cells

MDA-MB-231 (HTB-26™) cells from the ATCC were seeded adherently inside a sterile Airtech laminar flow safety cabinet (biosafety level 2) before being transferred into a sterile CO_2 air-jacketed incubator. In the safety cabinet, protection was provided using HEPA (high-efficiency particulate air) filters. The MDA-MB-231 (HTB-26™) cells were maintained in DMEM containing 10% foetal bovine serum (FBS) and were grown as monolayer cultures at 37°C in 5% CO_2 in T-25cm^3 sterile cell culture flasks in an atmosphere of 5% CO_2 and 95% humidified air (Figure 3.1). Once 70% confluency was reached, the cells were trypsinized and counted using an automated cell counter TC20. After the cell count, the cells were sub-cultured with 1 ml cell suspension and transferred to a T-25cm^3 culture flask containing 4 ml complete medium and stock cultures were maintained.

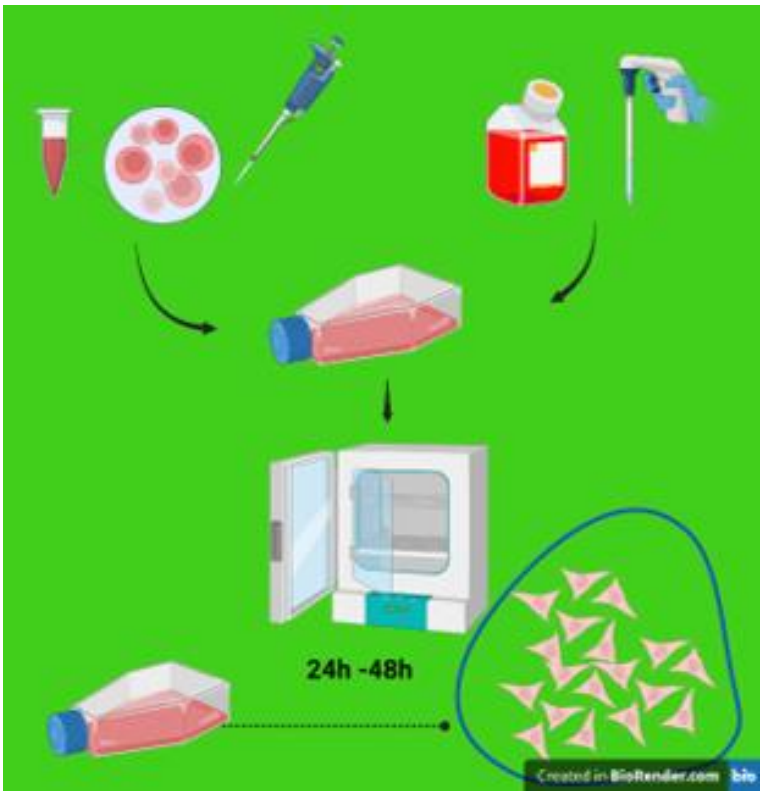

Figure 3.1: Cell culture and maintenance of 2D MDA-MB-231 cells. (Created with BioRender.com)

3.4.2 2D MDA-MB-231 cytotoxicity assay

The 3-(4,5-dimethylthiazol-2-yl)-2,5-diphenyl-2H-tetrazolium bromide, often known as the MTT reagent, is a mono-tetrazolium salt made up of three aromatic rings – two of which are phenyl moieties and one of which is thiazolyl – encircling a positively charged quaternary tetrazole ring core with four nitrogen atoms. When MTT is reduced, the central tetrazole ring is disrupted, and formazan, a violet-blue, water-insoluble molecule, is formed (Ghasemi et al., 2021). The MTT reagent is converted to formazan by metabolically active cells and may cross both the cell membrane and the inner membrane of the mitochondria in live cells, most probably because of its lipophilic nature and positive charge. The MTT assay was created by Mosmann et al. in 1983 as a colourimetric method of measuring intracellular formazan synthesis due to the chromogenic nature of this redox chemical reaction. As such, the assay's use as a cell metabolic activity assay is broad. It

has, however, been used more and more to infer unsupported secondary processes or cell states, such as viability (Ghasemi et al., 2021).

For the MTT assay, 1x 10^4 cells per well were seeded in 96-well plates and incubated at 37°C, 5% CO_2 and 95% humidified air for 24 h to enable cell adhesion. Subsequently, the medium was substituted with 200 µl culture medium containing doxorubicin at different concentrations, marking the 0 h time point. The assay was conducted after a total exposure time of 48 h. The following controls were used: untreated controls (to represent 100% viability) and dimethyl sulfoxide (DMSO) blank control wells (where cells treated with DMSO served as the vehicle control).

The doxorubicin stock solution was made in DMSO and kept at a temperature ranging from 2 to 8°C. Before administration, an aliquot of the stock solution was diluted to a 10-fold concentration range of 0.01-1000 µM using culture medium. After 48 h exposure, the medium was discarded from all the wells. Thereafter, 100 µl of non-additive medium was added to all the wells. The MTT stock solution of 5mg/ml was added to each well volume of 20 µl. The plate was covered and incubated for 3 h at 37°C. Following incubation, the content of each well was aspirated, and 50 µl of DMSO was added to each well to dissolve the formazan crystals. The plate was shaken on a shaker for 25 min. The quantity of formed formazan crystals in each well was determined by measuring absorbance at 560 nm, with a reference background wavelength of 630 nm, using a GloMax® Discover Microplate reader. The microplate reader measures the optical density (OD) of the homogenised MTT-formazan solution at a wavelength (about 570 nm) at which the formazan formed from MTT absorbs the most, hence reducing the transmission of light by absorbance and other mechanisms. It is considered that the measured OD values represent the formazan concentration and, in turn, the intracellular reduction of MTT (Ghasemi et al., 2021).

The calculated IC_{50} (the drug concentration causing 50% growth inhibition) for the drug-sensitive cells (MDA-MB-231 Wild-Type) was determined.

The absorbance values measured for each group were converted into relative percentage viability of the cells compared to the untreated control cells, using Equation (1),

$$\%Cell\ viability = \frac{(\Delta sample - \Delta blank)}{(\Delta untreated\ control - \Delta blank)} \times 100$$

where 'Δ sample' represents the difference between the value at 560 nm and the background value at 630 nm for all sample groups on the plate; 'Δ blank' denotes the difference between the value at 560 nm and the background value at 630 nm for the DMSO control wells; and 'Δ untreated' control signifies the difference between the value at 560 nm and the background value at 630 nm for the untreated control group.

Thereafter, Equation (2) was used to determine the relative percentage of cell viability inhibition (IC).

$$\%IC = 100\% - \%cell\ viability$$

3.4.3 Drug resistance induction of 2D MDA-MB-231 cell lines

The drug-resistant cell model was developed in the laboratory by repeatedly exposing the cancer cells growing in cell culture to doxorubicin. MDA-MB-231 Wild-Type cells were exposed to the antineoplastic agent, doxorubicin and maintained at a concentration range of IC_{10}-IC_{50} as calculated with the MTT assay using the MDA-MB-231 Wild-Type cells, for nine months. The IC_{50} of the surviving daughter cells was calculated, and a resistant clonal cell population (MDA-MB-231- DoxR) was developed. The IC_{50} was used to calculate the fold resistance between parental MDA-MB-231 Wild-Type cells and drug-resistant MDA-MB-231- DoxR cells using the following equation (McDermott et al., 2014):

Fold resistance = IC_{50} of resistant cell line/IC_{50} of parental (Wild-Type) cell line.

3.4.4 3D spheroid growth

This section describes the process of preparing the ClinoReactors™ for seeding and the sorting and sampling process of the spheroids before characterising. It also includes the steps taken to characterise the spheroids and the parameters used to characterise the spheroids.

3.4.4.1 Preparing the ClinoReactors™

Eight ClinoReactors™ were prepared 24 h before adding the cell suspension. Sterile distilled water was added to the humidity chambers. The cell chambers were washed with sterile distilled water and subsequently filled with 5 ml of non-additive culture medium. The ClinoReactors™ were inserted into the ClinoStar™ system (CelVivo™ ApS) to rotate and equilibrate overnight at a rotation speed of 15 rotations per minute (rpm) at 37°C, 5% CO_2 and 95% humidified air. After 24 h, the media were removed from the eight equilibrated ClinoReactors™. Then, the chamber was filled with 5 ml of fresh medium containing 0,5 µg/ml ascorbic acid (Vitamin C). A function of ascorbic acid is to influence the ECM by folding and depositing collagen proteins. The spheroids' complete health and structure creation were enhanced by increased ECM production (van Niekerk et al., 2023).

3.4.4.2 Preparing the spheroids for single-cell suspension

The single-cell suspension for seeding of drug-resistant MDA-MB-231 cells was obtained by trypsinization of the 2D doxorubicin-resistant TNBC MDA-MB-231 adherent cells (Figure 3.3 A). The number of viable cells in suspension was determined with an automated Sceptor 2.0 cell counter (Millipore, Massachusetts, USA).

A single-cell suspension with 1,2 x 10^6 cells was transferred to each of the equilibrated ClinoReactors™ (Figure 3.3 B). The ClinoReactors™ were then slowly filled with the medium without disturbing the cells. Cell culture medium should be visible in the top collar. The air bubbles trapped in the cell culture chamber were removed by gently tapping the ClinoReactors™. The area around the plug was sterilised with a 70% ethanol solution. The ClinoReactors™ were then placed into the ClinoStar™ system (Figure 3.3 C) and incubated at 37°C, 5% CO_2 and with an initial rotation of 2.5 rpm. The velocity was adjusted daily to compensate for spheroid growth. The media was changed for the first time after 72 h, then changed again after every 48 h. After seven days in culture, the spheroids in each of the eight ClinoReactors™ were sorted. The sorting process involved removing 180 spheroids from the equilibrated ClinoReactors™ and transferring them into each of four new ClinoReactors™, as shown in Figure 3.2. The four new ClinoReactors™ (technical replicates) were separated into two biological groups (1 and

2). The four new ClinoReactors™ with the spheroids were set into the ClinoStar™ system, starting at a rotational velocity of 14.4 rpm. Ideal conditions for growth were established through bi-daily changes in the growth medium and by modifying the rotational velocity to accommodate the growth of spheroids.

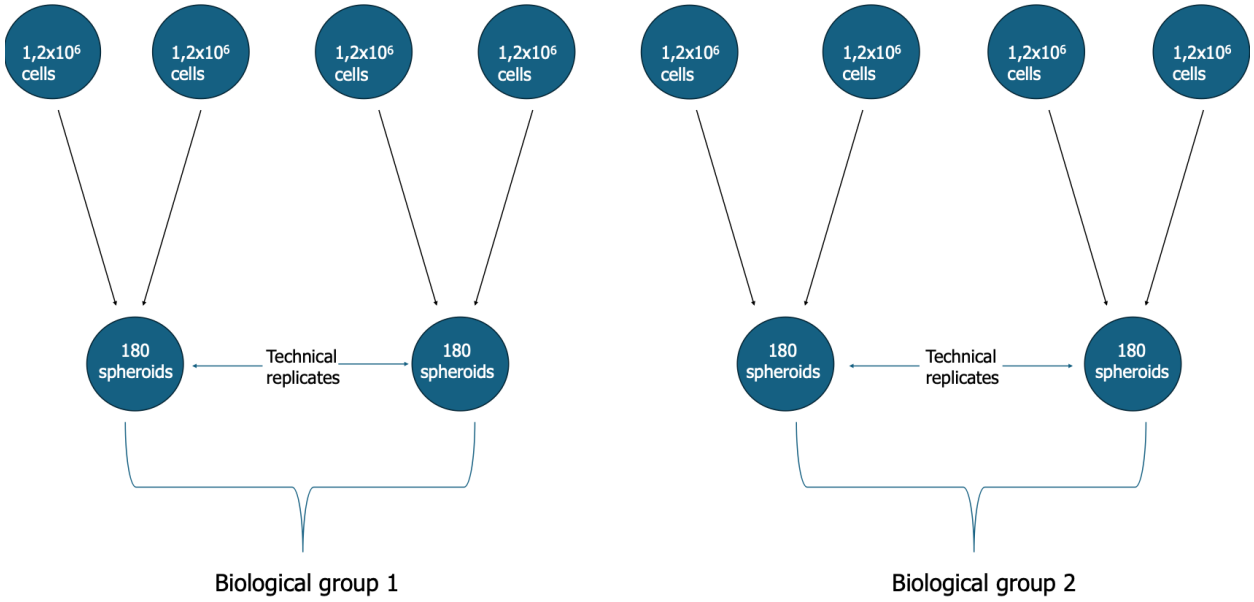

Figure 3.2: Illustration of ClinoReactor™ set up for characterisation. The first row represents the eight ClinoReactors™ with the single suspension with a density of 1,2x10^6 cells. The second row represents the two biological groups, each with two technical replicates obtained after sorting and placing 180 formed spheroids in each of the four ClinoReactors™

3.4.5 Characterisation of the MDA-MB-231 spheroid model

The number of days in culture where the spheroids reached metabolic equilibrium was determined to identify the optimal experimental window of the spheroid model. The parameters assessed comprised soluble protein content, intracellular ATP levels, estimated glucose consumption, planimetry of sampled spheroids, and extracellular AK

levels. To do this, the spheroids were sampled every other day until day 27 of culture, according to the aforementioned parameters. On day seven in culture, after sorting, the sampling process commenced. Sampling of the spheroids entailed the removal of 12 spheroids from one of the two ClinoReactors™ in each of the biological groups: two biological groups (four ClinoReactors™ in total), consisting of two technical replicates each. Sampling of spheroids occurred every other day from alternating technical replicates until day 27 in culture. For instance, on day nine, 12 spheroids were collected from ClinoReactors™ one and three each; on day 11, 12 spheroids were collected from ClinoReactors™ two and four each. Characterisation continued until day 27. Each spheroid was considered an autonomous unit that developed and adjusted independently. In total, 12 spheroids (six spheroids from each set of technical replicates) were selected for the intracellular ATP assay and 12 spheroids for the soluble protein assay, with two spheroids pooled together per well for each (n = 6). A total of 200 µL of the used medium was collected per technical replicate for the extracellular AK assay (Figure 3.3 E). The leftover medium was utilised to measure both glucose content and pH. Each measurement was conducted in duplicate (Figure 3.3 E). The characterisation parameters are discussed below.

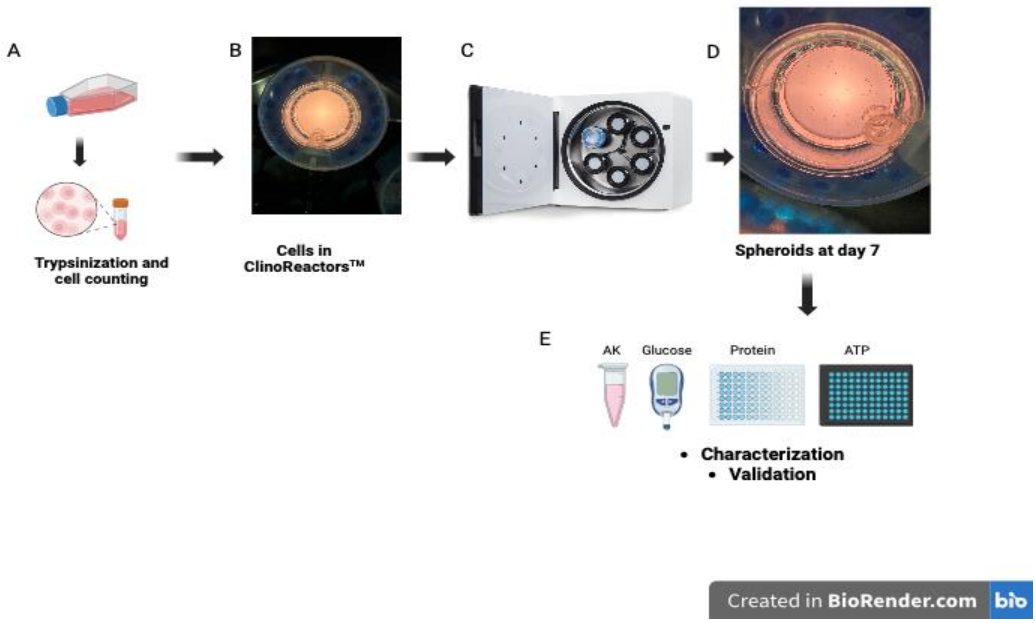

Figure 3.3: (A) Trypsinization and counting of two-dimensional cells. (B) Cells were added into ClinoReactors™ to form spheroids (cells are microscopic - nonvisible). (C) ClinoStar™ system. (D) Spheroids on day seven in culture (E) AK microtube, glucose monitor, ATP and protein plates for characterisation of spheroids. (Created with BioRender.com)

3.4.5.1 Planimetric determination of MDA-MB-231 spheroids

The planar surface area of the spheroids sampled was calculated using photomicrographs captured at 5x magnification. These images were taken from sampled spheroids from both the soluble protein assay and the intracellular ATP assay using a DFK 72AUCO2 USB 2.0 colour industrial camera (The Imaging Source, Bremen, Germany) linked to an inverted microscope (Nikon TS100/TS100F, Nikon Instruments, Tokyo) and the AxioVert A1 inverted transmitted light microscope with an Axiocam 305 mono fitted camera (195-043518) (Zeiss, Johannesburg, South Africa). The photomicrographs were transferred to image J software V1.53t (Java2HTML), and the 'shadow' area of spheroids was measured using the 'fitted polygon area' function, which calculates the planar surface of the spheroids in μm^2.

3.4.5.2 Soluble protein content

The protein content was determined using the Bradford assay. Six spheroids were sampled from one ClinoReactors™ per biological group, and two spheroids were pooled per well in clear 96-well plates. In total, there were six samples with six protein readings (three readings from each biological group). Twelve spheroids were sampled every 48 h prior to changing the culture medium to determine the soluble protein content using the Quick Start™ Bradford Protein assay (Bio-Rad, Lasec SA (Pty) Ltd, Midrand, South Africa). The sampled spheroids were lysed by adding 150 µl PBS and 10 µL lysis buffer to each well, and then 40 µl of protein assay dye reagent was added. The 96-well plate was then incubated at room temperature for 5 min. After centrifugation at 1 218 × *g* for 2 min, the absorbance was measured at 595 nm with a Spectramax® Paradigm plate reader. All samples were quantified against a bovine serum albumin (BSA) standard (Bio-Rad). The

protein content is a measure of cell growth but is also used to alter daily doses of treatment per protein content (Gouws et al., 2021).

3.4.5.3 Approximate glucose uptake assay

A volume of 20 µl of the cell culture medium was extracted from the ClinoReactors™ and transferred into a microcentrifuge tube. A OneTouch™ Vita glucose monitor and corresponding test strips were employed to measure the glucose concentration in the medium in triplicate, ensuring reproducibility. This assay is an indication of cell metabolic activity. As the cells die, less glucose is consumed from the growth medium. Glucose uptake was approximated relative to the fresh, unused culture medium glucose content.

3.4.5.4 Adenosine triphosphate (ATP) assay

Cell viability was measured based on the spheroids' ability to produce ATP. The CellTiter-Glo® Luminescent Cell Viability Assay and ATP standard (Sigma-Aldrich, Johannesburg, South Africa) was used according to the manufacturer's guidelines to determine the amount of ATP produced by the cells. Six spheroids were sampled from one ClinoReactor™ from each biological group. Two spheroids were pooled per well in a black 96-well plate, resulting in six ATP readings (n = 6). Every 48 hours, 12 spheroids were sampled in total. The transferred medium was removed from each well by making use of a pipette. A volume of 100 µl of PBS at room temperature was used to replace the growth medium, and thereafter, a volume of 100 µl CellTiter-Glo luminescent lysis buffer was introduced to each well-containing spheroids and PBS. Cell lysis was facilitated by the lysis buffer and repetitive gentle pipetting. The plate was covered with tin foil to protect it from light and placed onto a table shaker for 40 min at 300 rpm. Luminescence was measured on a Spectramax® Paradigm® plate reader (Fey and Wrzesinski, 2012).

3.4.5.5 Adenylate kinase (AK) assay.

AK is an important housekeeping enzyme that regulates cell energy balance by catalysing the reversible interconversion of ATP and AMP into two ADP molecules (Rogne et al., 2018). The cell membrane loses integrity during cell death, releasing the AK into the surrounding culture medium. Quantifying the extracellular AK relative to a known dead

cell control provides an indication of the number of dead cells in the culture. The ToxiLight™ BioAssay kit was used in a non-destructive assay, and healthy cells were not damaged. A volume of 200 µl of spent culture medium was sampled from one ClinoReactor™ per biological group in microcentrifuge tubes. The medium was centrifuged at 140 × *g* for 5 min, after which 160 µL of the supernatant was transferred to a new microcentrifuge tube. The transferred culture medium (140 µl) was subsequently centrifuged at 15,000 × *g* for 15 min, transferred to a new tube and snap frozen to be kept at -80°C until needed. Samples were adjusted between 20 and 22°C, and then 20 µl was plated per well in black 96-well plates with three technical replicates. Then 100 µl of AK detection reagent was added, and the covered plate was then set on a compact rocker for 20 min. The plate was then centrifuged at 1218 × *g* for 2 min, and the luminescence was measured with a Spectramax® Paradigm plate reader.

3.4.6 Reactivity of the MDA-MB-231 spheroid model to anti-cancer treatment

The reactivity of the MDA-MB-231 spheroid model to treatment was assessed with two different chemotherapeutic drugs, doxorubicin and cisplatin. The ClinoReactors™ were set up and maintained following the same procedures used for characterisation. On the seventh day of spheroid growth, 120 spheroids were introduced into each ClinoReactor™ (with two ClinoReactors™ assigned to each treatment group). Treatment commenced on day 15 of culture and was replaced every 24 hours after sampling over a 96 h period. Assays were conducted according to the procedures outlined in Section 3.4.4. The chemotherapeutic doses were determined according to the standard clinical doses given to patients diagnosed with TNBC: doxorubicin (60 mg/m^2) and cisplatin (75 mg/m^2) (Egelston et al., 2023, Rodler et al., 2023). A third treatment group was included: the calculated doxorubicin IC_{50} dose obtained from MTT results from 2D cell culture treatment. The human body's protein constitutes approximately 14 to 16% of the total body weight (Duda et al., 2019). The dosages of both chemotherapeutic drugs (clinical and IC_{50}) were calculated by assessing the soluble protein (biomass) of the spheroids in

each ClinoReactor™ daily, following sampling and prior to treatment, modifying the chemotherapy dose correspondingly. An untreated control group was also included.

3.5 STATISTICAL DATA ANALYSIS

Data analysis for the cytotoxicity assays was performed using non-linear regression analysis to determine the best-fit IC_{50} estimates, with a corresponding 95% confidence interval (95% CI) for doxorubicin, using the [inhibitor] vs normalised response – variable slope template of GraphPad Prism (GraphPad Prism version 10.1.3 for Windows, GraphPad Software, San Diego California USA). Data analysis was performed with GraphPad Prism (GraphPad Prism version 9 for Windows, GraphPad Software, San Diego, California, USA). Statistical analysis was conducted on the collected data to detect significant differences between the untreated control group and the experimental groups by using Dunnett's multiple comparison test. Differences were deemed statistically significant when $p \leq 0.05$.

CHAPTER FOUR

4.0 RESULTS

4.1 MDA-MB-231 cytotoxicity assay

Gradually increasing concentrations of doxorubicin led to a dose-dependent reduction in cell viability, following a sigmoidal curve in both the Wild-Type cells (Figure 4.1 A) and doxorubicin-resistant cells (Figure 4.1 B). The sub-toxic concentrations of doxorubicin tested are provided in Table 4.1. An IC_{50} of 2,78 µM and 13,96 µM for the Wild-Type cells and doxorubicin-resistant cells, respectively, were determined.

Table 4.1: The IC_{50} values of doxorubicin determined for the Wild-Type cells and the doxorubicin-exposed MDA-MB-231 cells.

	MDA-MB-231 Wild-Type cell line	**MDA-MB-231 DoxR cell line**
IC_{50}	2,78 µM	13,96 µM

Fold resistance = IC_{50} of resistant cell line/IC_{50} of Wild-Type cell line.

=13,96 µM /2,78 µM

= 5,01

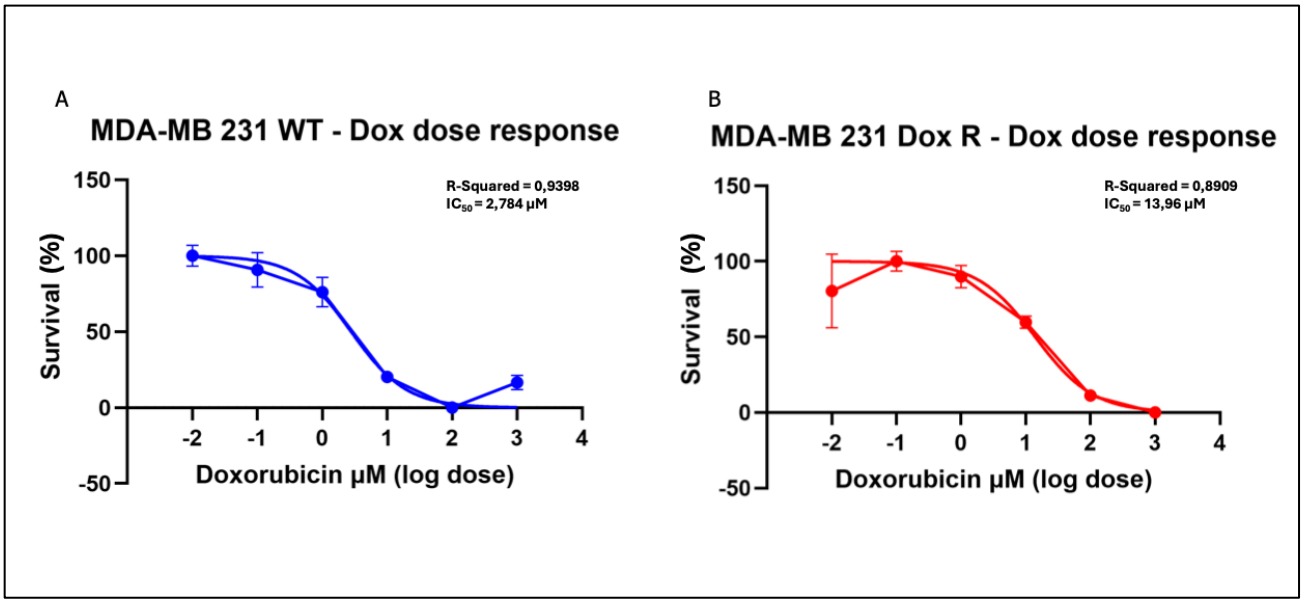

Figure 4.1: Dose-response curves showing MDA-MB-231 cell survival following treatment with increasing log dosages from 0,01 - 100 µM doxorubicin for 48 h. (A) Wild-Type, and (B) doxorubicin exposed cells (n = 8). The IC_{50} was calculated using a non-linear regression curve fit (log[inhibitor] vs response) with a robust fit.

Doxorubicin elicited a cytotoxic response on monolayers at the concentrations, as indicated by the dose-response curves in Figure 4.1. The IC_{50} for the doxorubicin-exposed cells was higher than that of the Wild-Type cells due to them having been exposed to doxorubicin for a prolonged period. This continued exposure to doxorubicin has resulted in the cells acquiring resistance to treatment compared to the Wild-Type cells.

4.2 MDA-MB-231 DoxR spheroid model for characterisation

MDA-MB-231 DoxR spheroids were initiated using the single-cell suspension method whereby a single-cell suspension was transferred into ClinoReactors™ and rotated slowly to allow natural aggregation into spheroids. From day seven until day 27 in culture, the spheroids' viability and growth were assessed by measuring soluble protein levels, intracellular ATP content, approximate glucose consumption, surface area, and the release of extracellular AK. The spheroids' viability and metabolic stability over 27 days

were determined to assess if the MDA-MB-231 DoxR spheroids could be valuable for in vitro drug screening evaluations in TNBC.

4.2.1 Planimetry

By day 7 in culture, the spheroids were successfully formed. However, the typical compact and smooth structure expected was not observed. The spheroids were maintained until day 27 (Figure 4.2 A-E). The spheroid size was determined between day 7 and day 27 by evaluating the surface area. The average spheroid size (Figure 4.3(a)) decreased between day 7 (85889,00 μm^2) and day 11 (50460,00 μm^2), which suggests that the spheroids could be compacting if they were not losing viability simultaneously. The spheroid size then increased between day 11 and day 19 (86171,50 μm^2), suggesting that cells on the outer layer of the spheroids were proliferating, resulting in the growth of the spheroids. Spheroid size decreased on day 25 (75864,80 μm^2) and day 27 (44153,18 μm^2), potentially indicating loss of viability.

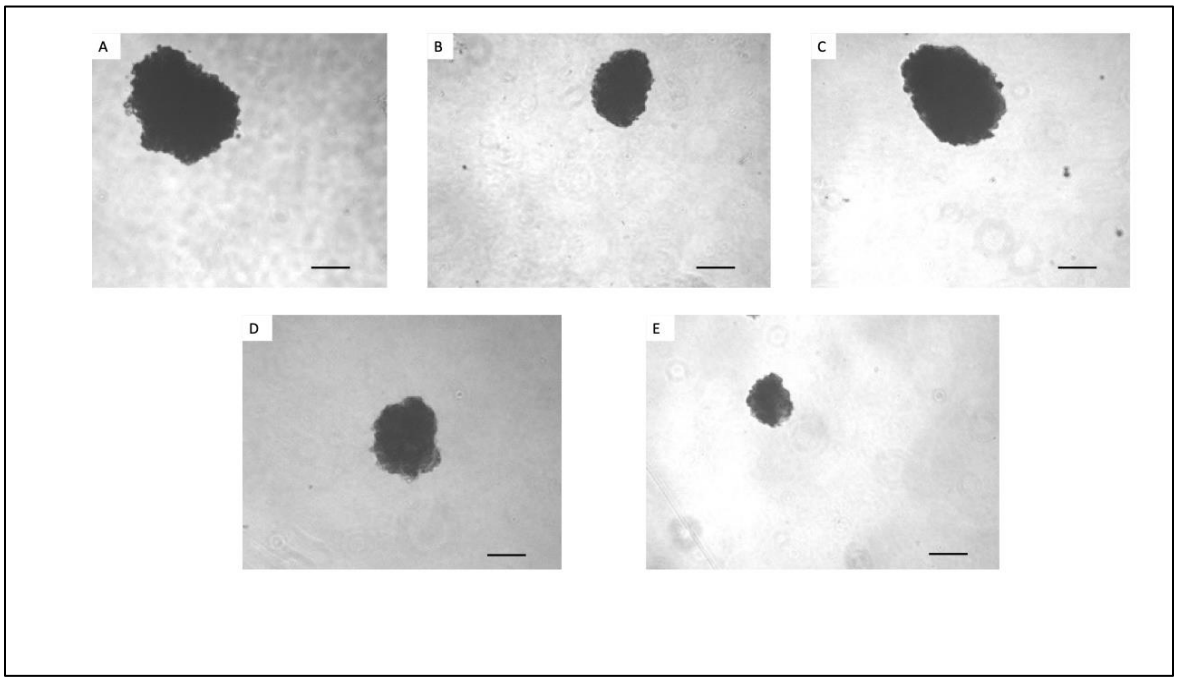

Figure 4.2: Phase contrast images of the MDA-MB-231 DoxR spheroids grown in ClinoReactors™ using the single cell suspension method on day 7 (A), day 11 (B) day

19(C), day 25 (D) and day 27 (E). Images captured using a 5x objective; scale bars = 200 µm).

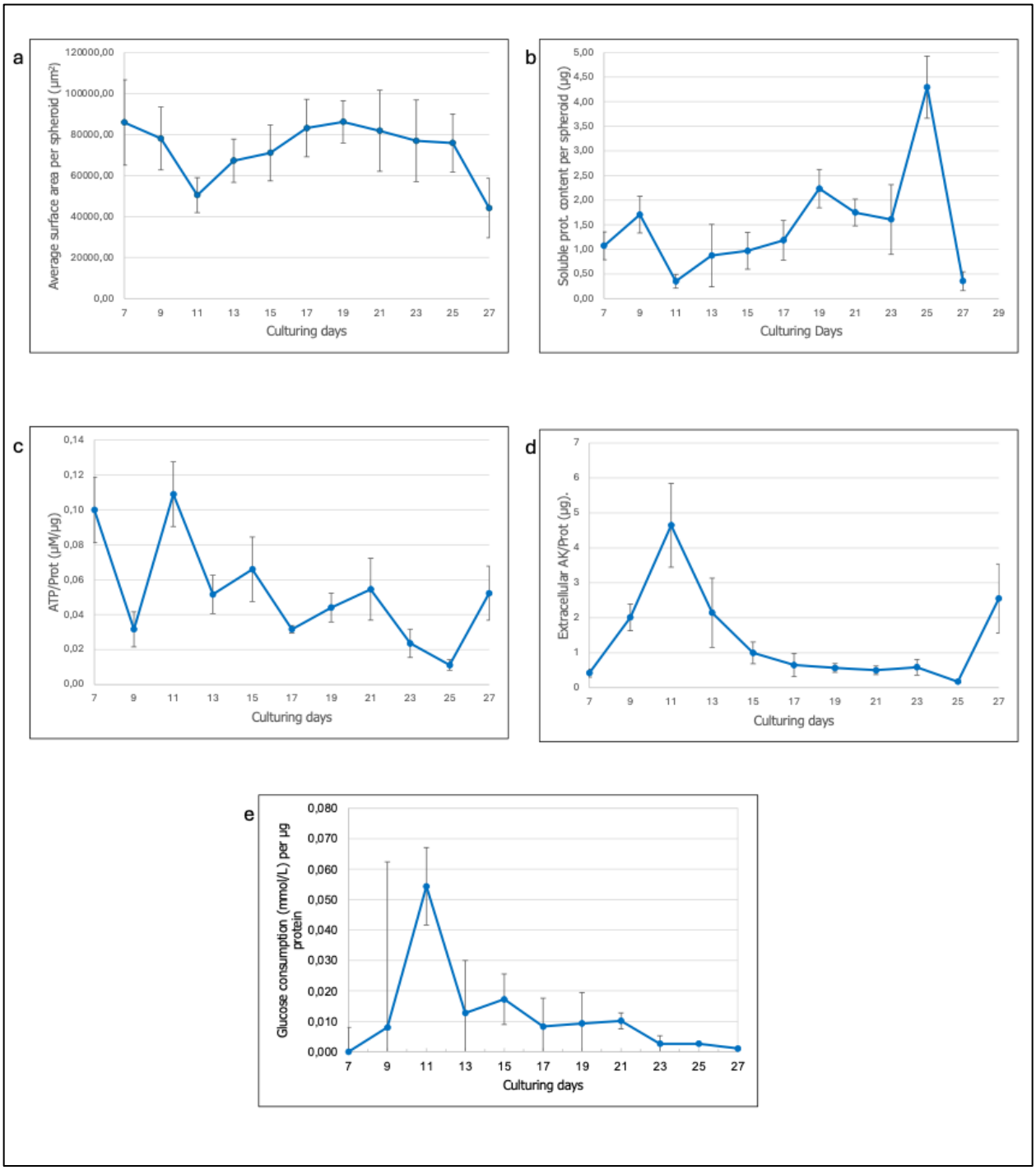

Figure 4.3: Characterisation of the MDA-MB-231 DoxR spheroid model as a function of time in terms of (a) average planar surface area per spheroid (μm^2); (b) soluble protein content per spheroid (μg); (c) intracellular adenosine triphosphate content per soluble protein (μM/μg); (d) extracellular adenylate kinase release per μg protein; and (e) approximate glucose consumption (mmol/L) per μg protein. Error bars = standard deviation (n = 6).

4.2.2 Soluble protein content

Protein content was used as an indicator to determine if the growth of the spheroids observed correlated with an increase in cell number. There was an increase in protein content from day 11(0,35 μg) to day 19 (2,23 μg), as indicated in Figure 4.3(b), which correlates with the observed increase in spheroid size between these days. This suggests that protein content increased due to an increase in cell number. The protein content decreased slightly between day 21 (1,75 μg) and day 23 (1,61 μg), which also corresponds with the observed slight decrease in spheroid size. Protein content spiked at day 25 (4,30 μg). However, this was probably due to a pipetting error. The protein content then decreased markedly by day 27 (0,35 μg), similar to the marked decrease in size, suggesting loss of viability and increased cell death.

4.2.3 Intracellular ATP

The MDA-MB-231 DoxR intracellular ATP content of spheroids was normalised relative to protein content to account for both spheroid development and cell density changes due to sampling (Figure 4.3(c)). The ATP produced by the cells was measured over a period of 27 days, which indicates the cells' metabolic activity. ATP levels fluctuated between day 7 (0,10 μM/μg) and day 13 (0,05 μM/μg). There was an increase in the ATP values on day 15 (0,07 μM/μg); however, it decreased by day 17 (0,03 μM/μg) due to an experimental error, where the spheroids broke apart during a medium change. The spheroids were then replaced with healthy spheroids, and from day 19 (0,04 μM/μg) to day 21 (0,05 μM/μg), the ATP values increased again. ATP levels began to decrease

continuously from day 21 to day 25 (0,01 µM/µg), which supports the previously suggested loss of cell viability of the spheroids.

4.2.4 Extracellular adenylate kinase

The AK released per protein increased markedly between day 7 (0,41 per µg protein) and day 11 (4,64 per µg protein) (Figure 4.3(d)), which suggests that the spheroids were still adapting to their environment and were potentially stressed from the handling. AK then decreased from day 11 to day 17 (0,64 per µg protein); and from day 17, the AK levels were relatively low and stable until day 23 (0,58 per µg protein). The AK level then decreased slightly on day 25 (0,17 per µg protein) before rapidly increasing by day 27 (2,55 per µg protein). This again supports the suggested loss of spheroid viability and increased cell death.

4.2.5 Approximate glucose uptake

Approximate glucose uptake by spheroids is an indication of cellular metabolic activity. As the cells die, they are less metabolically active. Therefore, less glucose is consumed from the growth medium. On day 7, following spheroid sorting, fresh medium was introduced into each ClinoReactors™. This value was considered the initial glucose measurement (21,1 mmol/L on average (n=4)) present in each ClinoReactors™. The difference between the glucose content in the used medium of each ClinoReactor™ and the mean glucose content of the new culture medium was calculated to estimate the approximate glucose consumed per ClinoReactor™. To adjust for biomass, glucose consumption was normalised against to the total protein content in each ClinoReactor™ (number of spheroids × protein content per spheroid), yielding glucose consumption per protein. The glucose content increased from day 9 (0,008 mmol/L) to day 11 (0,054 mmol/L), as indicated in Figure 4.3(e). Glucose content decreased on day 13 (0,013 mmol/L), followed by a slight increase on day 15 (0,017 mmol/L). Glucose consumption remained relatively constant until a constant decrease could be observed from day 23 to

day 27, suggesting reduced metabolic activity of the spheroids during this period, thus consuming less glucose. This trend is supported by the ATP/protein data between day 13 to day 21. The data indicates that the spheroids maintained metabolic activity throughout the 27-day culture period.

4.3 Qualification of the MDA-MB-231 DoxR spheroid for treatment evaluation

To assess the suitability of the MDA-MB-231 DoxR spheroid model for screening anti-cancer treatment activities, its response to conventional chemotherapeutic treatments was assessed. Two model drugs, doxorubicin and cisplatin, were employed for this purpose. The treatments were applied to the spheroid groups at clinical doses typically used for treating TNBC patients and the doxorubicin IC_{50} for a 96 h period. As described earlier, the dosages were converted to treatment per µg protein of the spheroids. All data were normalised against the untreated control group. The procedures for initiating and maintaining spheroids identical to those used for model characterisation were employed to evaluate the treatments. On day 7 of culturing, spheroids were sorted, counted, and readied for treatment. Treatment commenced at day 15 (0 h). Sampling of spheroids occurred every 24 h over a period of 96 h. The medium comprising the drug and 0.5 µg/ml of Vitamin C were replaced every 24 hours after sampling. Daily treatment dosages were adjusted based on the biomass still present in each ClinoReactor™.

The dosages per protein were as follows:

Cisplatin clinical dose = $4{,}435 \times 10^{-6}$ µg/µg protein

Doxorubicin clinical dose = $1{,}064 \times 10^{-5}$ µg/µg protein

Doxorubicin [IC_{50}] = $7{,}8 \times 10^{-2}$ µg/µg protein

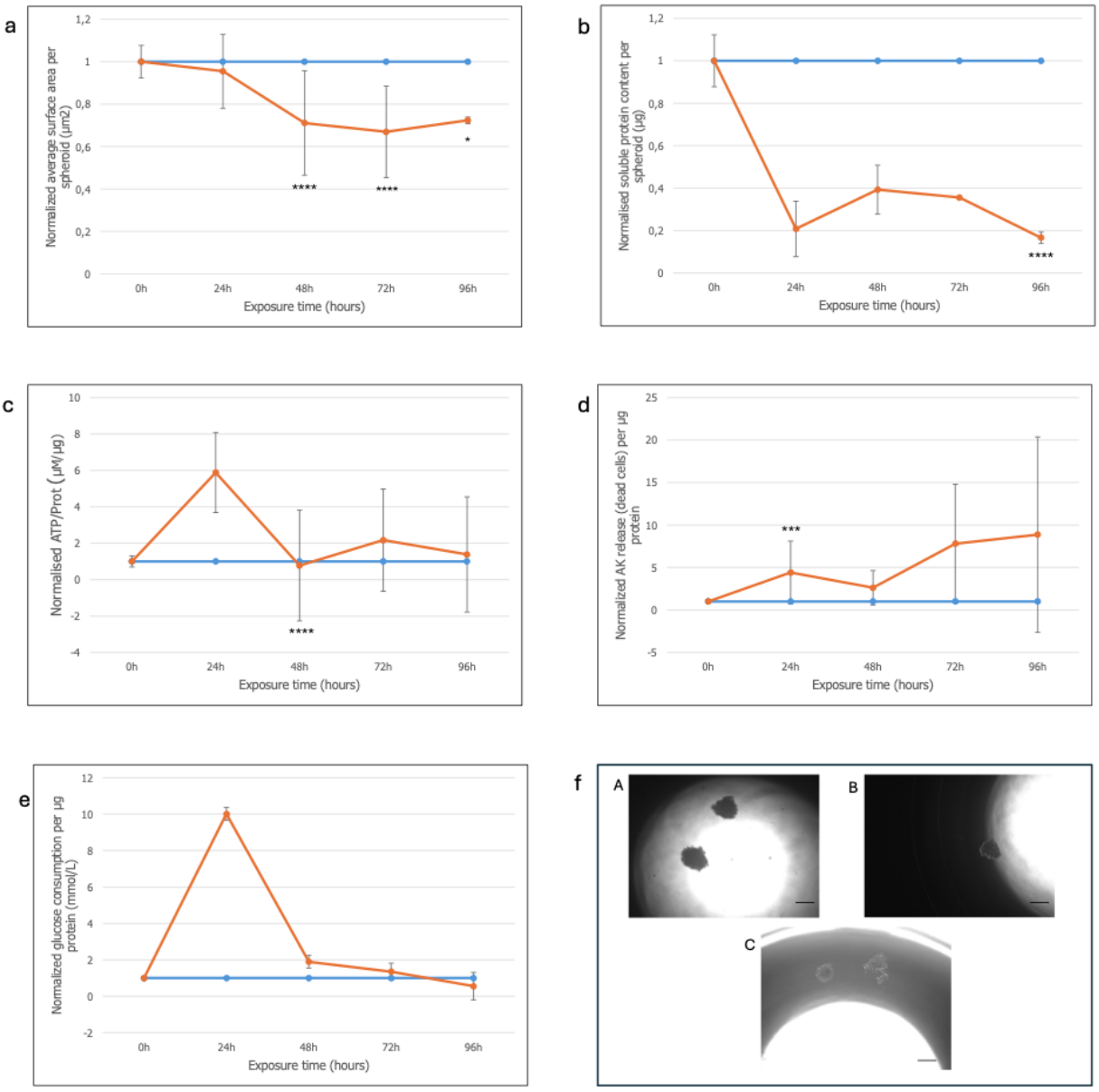
a
Normalized average surface area per spheroid (µm2)
1,2
1
0,8
0,6
0,4
0,2
0
0h
24h
48h
72h
96h
Exposure time (hours)
****
****
*
b
Normalised soluble protein content per spheroid (µg)
1,2
1
0,8
0,6
0,4
0,2
0
0h
24h
48h
72h
96h
Exposure time (hours)
****
c
Normalised ATP/Prot (µW/µg)
10
8
6
4
2
0
-2
-4
0h
24h
48h
72h
96h
Exposure time (hours)
****
d
Normalized AK release (dead cells) per µg protein
25
20
15
10
5
0
-5
0h
24h
48h
72h
96h
Exposure time (hours)
***
e
Normalized glucose consumption per µg protein (mmol/L)
12
10
8
6
4
2
0
-2
0h
24h
48h
72h
96h
Exposure time (hours)
f
A
B
C

Figure 4.4: Evaluation of the MDA-MB-231 DoxR spheroid model growth and viability following treatment with a clinical dose of cisplatin for 96 h, as a function of time, in terms of (a) average planar surface area per spheroid (μm^2); (b) soluble protein content per spheroid (μg); (c) intracellular adenosine triphosphate content per soluble protein (μM/μg); (d) extracellular adenylate kinase release per μg protein; and (e) approximate glucose consumption (mmol/L) per μg protein. The blue line represents the normalised untreated control group, while the orange line represents the cisplatin-treated group. (f) Photomicrographs of the group treated with cisplatin after (A) 0 h, (B) 48 h, and (C) 96 h (scale bar = 200 μm) are shown as (f). Data was normalised relative to the untreated control group. Error bars = standard deviation (n = 6). *Statistically significant difference: $p \leq 0.05$ (one-way ANOVA followed by Dunnetts's multiple comparison test for comparison with the untreated control).

4.3.1 Cisplatin clinical dose treatment

Treatment with a clinical dose of cisplatin (4,435 x 10^{-6} μg/μg protein) for 24 h slightly decreased the planar surface area (0,95 μm^2 per spheroid) of the MDA-MB-231 DoxR spheroids and significantly decreased the soluble protein content to an average of 0,21 μg per spheroid at the same time point as observed in Figures 4.4 (a) and (b), respectively. The planar surface area of the spheroids dramatically reduced after 48 h of treatment with a recorded average diameter of 0,71 μm^2 (p<0.0001) per spheroid, whilst the soluble protein content slightly increased at that time point to an average of 0,40 μg per spheroid. Planar surface area remained significantly decreased after 72 h (0,67) μm^2 per spheroid) (p<0.0001) and 96 h (0,72 μm^2 per spheroid) (p=0.0361) of treatment. The soluble protein content also remained lower, relative to the untreated control, following 72 h of treatment (0,35 μg per spheroid) and further decreased significantly (p=0.0004) after 96 h to an average of 0,17 μg per spheroid. Cisplatin appeared to greatly influence spheroid growth as both planar surface area and soluble protein content were significantly lower than in the untreated control following exposure to the drug.

The normalised ATP/protein (μM/μg), plotted as a function of time, is shown in Figure 4.4(c). There was an increase in ATP levels following 24 h of exposure to cisplatin,

followed by a statistically significant decrease (p<0.0001) after 48 h of treatment. ATP levels were similar to or higher than those in the untreated control group, suggesting that the cells were still alive and producing ATP. There was a slight increase after 72 h followed by a slight decrease after 96 h of treatment; however, the ATP levels were still higher than in the untreated control group, which suggests the presence of viable and metabolically active cells. Extracellular AK per protein showed a corresponding statistically significant increase (p=0.0004) following 24 h exposure to cisplatin (Figure 4.4(d)). This increase in cell death is corroborated by the concurrent reduction in spheroid size. The simultaneous increase in AK and ATP might suggest the occurrence of apoptosis (Calitz et al., 2018). AK levels continued to rise until 96 h of treatment, signalling ongoing cell death. This observation is reinforced by the decline in glucose consumption after 48 h (Figure 4.4(e)), suggesting fewer metabolically active cells were present. The above data suggests that the spheroids were highly sensitive to cisplatin treatment. Furthermore, as observed in Figure 4.4(f), cisplatin treatment significantly affected spheroid size and structural integrity.

While there was a noticeable increase in cell death at the 48 h, 72 h, and 96 h time points relative to the untreated control, no statistical significance was observed, likely due to the large standard deviations observed. These deviations could be attributed to spheroid integrity loss from treatment and variations in spheroid sizes due to frequent handling during sampling. The increased cell death resulted in more debris in the culture media, potentially affecting the AK analysis. For the AK assay, media from the ClinoReactors™ is sampled and centrifuged to remove cells to ensure only extracellular AK is measured. However, because the spheroids start to break apart and cells deteriorate from treatment, as observed in Figure 4.4 (f-C), removing all cell debris and damaged cells during centrifugation becomes a challenge. Larger variations in AK values are, therefore, a drawback of the assay. The lack of such large standard deviations for the other assays highlights that the spheroid samples themselves were not much different, and the issue was assay-specific.

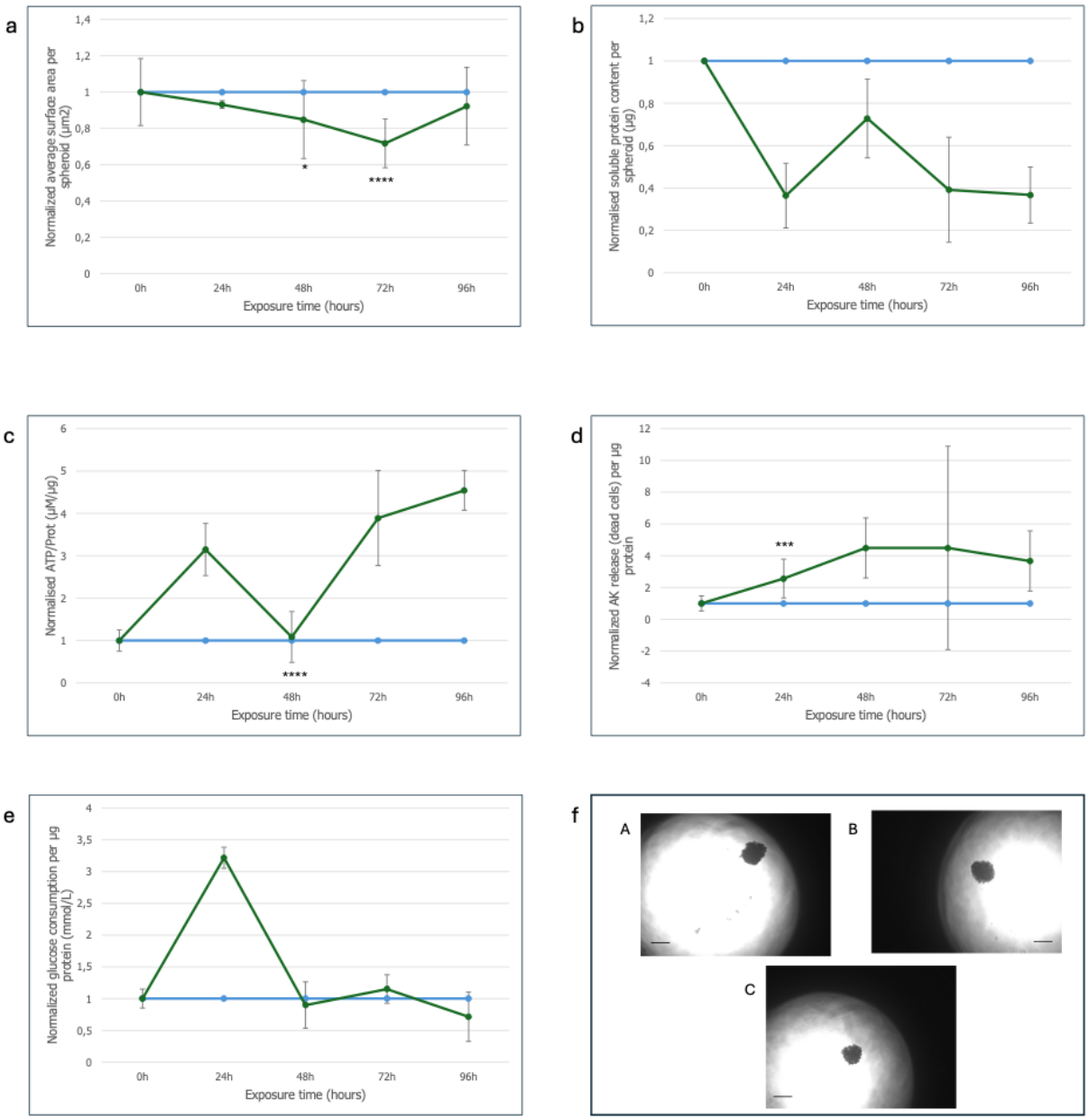
a
Normalized average surface area per spheroid (µm2)
1,4
1,2
1
0,8
0,6
0,4
0,2
0
*
****
0h
24h
48h
72h
96h
Exposure time (hours)
b
Normalised soluble protein content per spheroid (µg)
1,2
1
0,8
0,6
0,4
0,2
0
0h
24h
48h
72h
96h
Exposure time (hours)
c
Normalised ATP/Prot (µM/µg)
6
5
4
3
2
1
0
****
0h
24h
48h
72h
96h
Exposure time (hours)
d
Normalized AK release (dead cells) per µg protein
12
10
8
6
4
2
0
-2
-4
***
0h
24h
48h
72h
96h
Exposure time (hours)
e
Normalized glucose consumption per µg protein (mmol/L)
4
3,5
3
2,5
2
1,5
1
0,5
0
0h
24h
48h
72h
96h
Exposure time (hours)
f
A
B
C

Figure 4.5: Evaluation of the MDA-MB-231 DoxR spheroid model growth and viability following treatment with a clinical dose of doxorubicin for 96 h, as a function of time, in terms of (a) average planar surface area per spheroid (μm^2); (b) soluble protein content per spheroid (μg); (c) intracellular adenosine triphosphate content per soluble protein (μM/μg); (d) extracellular adenylate kinase release per μg protein; and (e) approximate glucose consumption (mmol/L) per μg protein. The blue line represents the normalised untreated control group, while the green line represents the doxorubicin-treated group. (f) Photomicrographs of the doxorubicin clinical dose-treated group after (A) 0 h, (B) 48 h, and (C) 96 h (scale bar = 200 μm) are shown as (f). Data was normalised relative to the untreated control group. Error bars = standard deviation (n = 6). *Statistically significant difference: $p \leq 0.05$ (one-way ANOVA followed by Dunnetts's multiple comparison test for comparison with the untreated control).

4.3.2 Doxorubicin clinical dose treatment

Doxorubicin slightly reduced the planar surface area following 24 h exposure (1,064 x 10^{-5} μg/μg protein) to an average of 0,93μm^2 per spheroid, as shown in Figure 4.5(a). It further decreased (0,84 μm^2 per spheroid) following 48 h of treatment (statistically significant, p=0.0164). However, the decrease was less significant than that of cisplatin treatment following 48 h of exposure. The planar surface area continued to decrease significantly (p<0.0001) following 72 h (0,72 μm^2 per spheroid) of treatment but recovered after 96 h of treatment (0,92 μm^2 per spheroid) to almost the same size as the untreated control, suggesting that the remaining cells were able to recover, at least to some extent. The soluble protein content decreased notably following 24 h of treatment to an average of 0,36 μg per spheroid, but this was again reduced to a smaller extent than that of the cisplatin-treated samples after 24 h exposure. The protein content recovered somewhat at 48 h (0,73 μg per spheroid) (Figure 4.5(b)) before decreasing again. It then remained stable between 72 h (0,39 μg per spheroid) and 96 h (0,37 μg per spheroid) of treatment.

Following 24 h exposure to a clinical dose of doxorubicin, the ATP/protein (μM/μg) increased, as shown in Figure 4.5(c), and then decreased at a statistically significant level (p<0.0001), to a similar level as that of the untreated control after 48 h of treatment. Following 72 h exposure, the ATP/protein increased again and continued to increase to the 96 h time point. Simultaneously, the levels of AK per protein showed a constant increase after initial exposure to doxorubicin (Figure 4.5 (d)), suggesting active cell death such as apoptosis. At 24 h of treatment, AK levels increased to a statistically significant level (p=0.0001) and remained elevated until 72 h of treatment. The increased AK levels for the doxorubicin clinical dose-treated group were still lower than for the cisplatin-treated group, indicating less extensive cell death. After 96 h of treatment, AK decreased slightly, which could suggest that the cells were recovering. This is supported by the increase in spheroid size at 96 h (Figure 4.5(a)). The increase in ATP after 24 h and 72 h of treatment coincides with an increase in glucose consumption, as shown in Figure 4.5(e) at those time points. This indicates the presence of metabolically active cells. In cancer cells, the synthesis of ATP and resistance to drugs are directly correlated. The most aggressive cancer cells are those with high ATP levels because they have stem-like characteristics that increase multidrug resistance and raise the potential for cell migration, spontaneous metastasis, and invasion. These cells are thought to resist both traditional chemotherapy's effects and a hostile microenvironment. Their high ATP content enables these cells to naturally select for survival, which encourages distant metastasis and tumour recurrence (van Niekerk et al., 2023). Visually, as observed in Figure 4.5(f), doxorubicin impacted spheroid size and structure much less than in the cisplatin treatment group. The spheroids maintained their structure and remained compact.

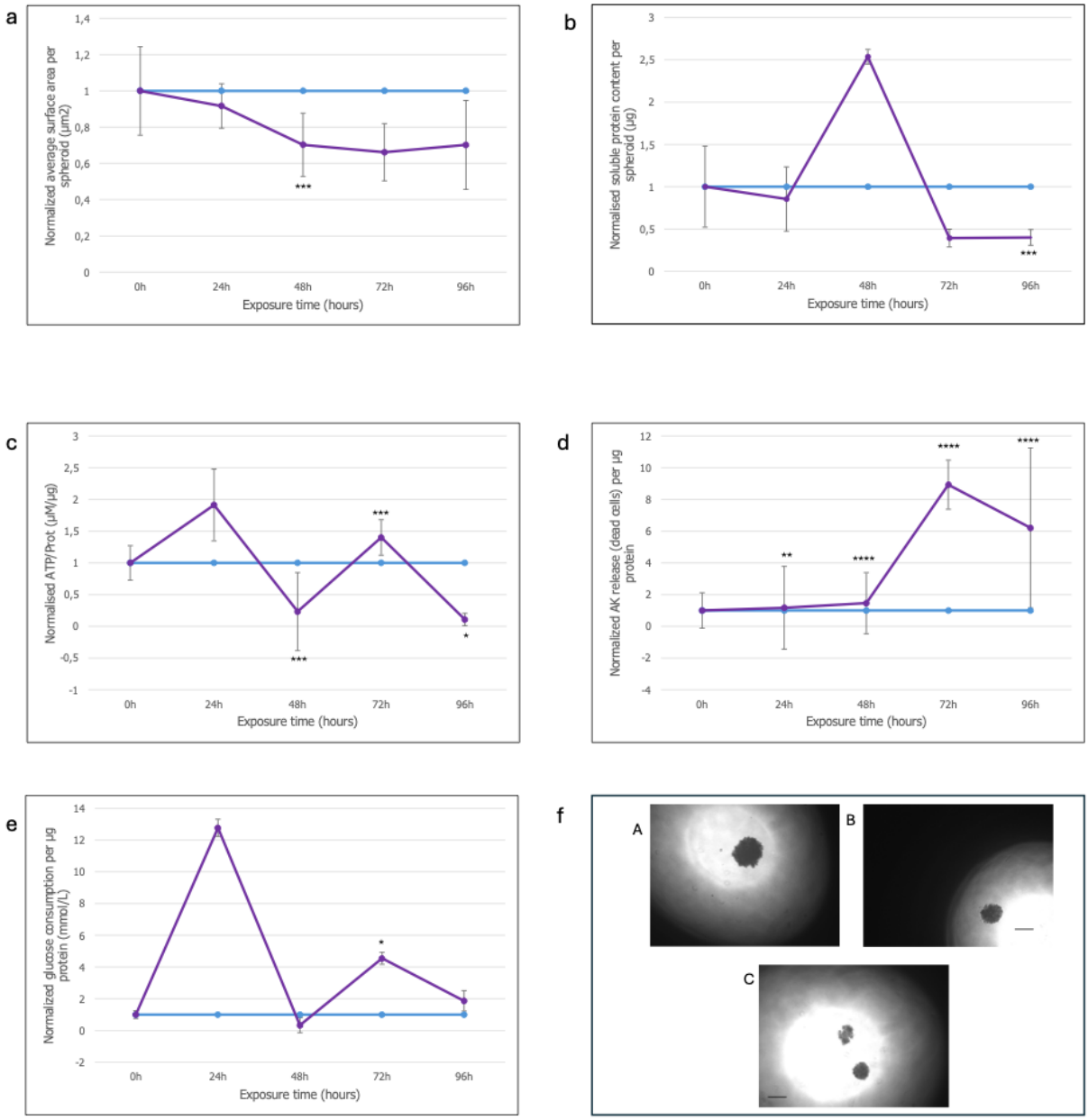
a
Normalized average surface area per spheroid (µm2)
1,4
1,2
1
0,8
0,6
0,4
0,2
0
***
0h
24h
48h
72h
96h
Exposure time (hours)
b
Normalised soluble protein content per spheroid (µg)
3
2,5
2
1,5
1
0,5
0
***
0h
24h
48h
72h
96h
Exposure time (hours)
c
Normalised ATP/Prot (µM/µg)
3
2,5
2
1,5
1
0,5
0
-0,5
-1
***
***
*
0h
24h
48h
72h
96h
Exposure time (hours)
d
Normalized AK release (dead cells) per µg protein
12
10
8
6
4
2
0
-2
-4
**
****
****
****
0h
24h
48h
72h
96h
Exposure time (hours)
e
Normalized glucose consumption per µg protein (mmol/L)
14
12
10
8
6
4
2
0
-2
*
0h
24h
48h
72h
96h
Exposure time (hours)
f
A
B
C

Figure 4.6: Evaluation of the MDA-MB-231 DoxR spheroid model growth and viability following treatment with the calculated doxorubicin IC_{50} concentration for 96 h, as a function of time, in terms of (a) average planar surface area per spheroid (μm^2); (b) soluble protein content per spheroid (µg); (c) intracellular adenosine triphosphate content per soluble protein (µM/µg); (d) extracellular adenylate kinase release per µg protein; and (e) approximate glucose consumption (mmol/L) per µg protein. The blue line represents the normalised untreated control group, while the purple line represents the doxorubicin IC_{50} treated group. (f) Photomicrographs of the doxorubicin IC_{50} treated group after (A) 0 h, (B) 48 h, and (C) 96 h (scale bar = 200 µm) are shown as (f). Data was normalised relative to the untreated control group. Error bars = standard deviation (n = 6). *Statistically significant difference: $p \leq 0.05$ (one-way ANOVA followed by Dunnetts's multiple comparison test for comparison with the untreated control).

4.3.3 Doxorubicin IC_{50} treatment

Exposure to the doxorubicin IC_{50}, which was in a higher concentration (7,8 x 10^{-2} µg/µg protein) than the doxorubicin clinical dose (1,064 x 10^{-5} µg/µg protein), follows the same trend as the cisplatin-treated group in terms of planar surface area (Figure 4.6 (a)). There was a slight decrease following 24 h of treatment (0,92 μm^2 per spheroid), followed by a further statistically significant decrease (p=0.0002) after 48 h of treatment (0,70 μm^2 per spheroid). Planar surface area remained relatively stable until 96 h exposure (0,70 μm^2 per spheroid). The soluble protein content followed the same trend with a gradual decrease, except for a notable spike after 48 h exposure (2,54 µg per spheroid), as shown in Figure 4.6 (b). The spike occurred due to a pipetting error, where less PBS was added to the wells, resulting in an exaggeration in the protein reading. Soluble protein content decreased to 0,39 µg per spheroid following 72 h of treatment and then to 0,40 µg per spheroid (p=0.0003) after 96 h of treatment. Doxorubicin IC_{50} had a notable impact on spheroid size and soluble protein content, and this impact was maintained without recovery. The effect was more pronounced than for the clinical dose doxorubicin treatment.

ATP/protein (µM/µg) levels increased after 24 h of treatment, as observed in Figure 4.6 (**c**); however, they then decreased significantly (p<0.0001) following 48 h of treatment. Although there was an increase in ATP/protein in the next 24 h, this could not be sustained, and the ATP levels decreased until 96 h of treatment, when ATP was almost depleted. Again, the effect of doxorubicin IC_{50} was much more pronounced than the clinical dose or even than the cisplatin clinical dose treatment.

AK per protein increased steadily during the initial 48 h of treatment (Figure 4.6 (d)). AK levels increased significantly after 48 h of treatment (p<0.0001), with the highest peak at 72 h. The measured cell death was again more pronounced than for the doxorubicin IC_{50}-treated group but was similar to that of the cisplatin-treated group. The simultaneous increase in ATP and AK levels at 72 h of treatment suggests that the cells were undergoing apoptosis, showing an energy-dependent mechanism of cell death. However, since ATP levels were almost depleted after 96 h of treatment, the high AK levels at 96 h of treatment suggest an energy-independent mechanism of cell death, such as necrosis.

Glucose consumption was elevated following 24 h of treatment (Figure 4.6 (e)). Glucose serves as the primary energy source for cellular metabolism. It is catabolised through three processes to produce ATP: glycolysis, the tricarboxylic acid cycle (TCA or Krebs cycle), and oxidative phosphorylation (Bonora et al., 2012). Glucose consumption decreased to just below that of the untreated control group at the 48 h timepoint. Consumption then increased significantly for the following 48 h, suggesting that many metabolically active cells were still present. However, the glucose was not converted to ATP. Visually, as observed in Figure 4.6 (f), doxorubicin IC_{50} treatment significantly affected the size and structure of the MDA-MB-231 DoxR spheroids. Some spheroids lost structural integrity, while some were able to maintain their structure, although they decreased in size.

CHAPTER FIVE

5.1 DISCUSSION

Chemo-resistance and inadequate testing procedures provide a significant obstacle to the effective chemotherapeutic treatment of TNBC. Another contributing factor is the utilisation of poorly representative pre-clinical models in *in vitro* anti-cancer drug screening and drug efficacy evaluation. These methods include 2D cell-based models and *in vivo* animal models as predictive models of human disease (Kitaeva et al., 2020). However, 2D cell-based models have several limitations. For example, 2D cells are grown as a monolayer, exposing them to equal amounts of nutrients and oxygen in the medium. This allows the cells to synchronise at the same cell cycle stage (Brancato et al., 2020, Ncube et al., 2023). This, however, is not the case *in situ.* Furthermore, because the penetration barrier that occurs in *in vivo* situations is not replicated, all cells cultured in a 2D configuration are subjected to identical drug concentrations. Consequently, it appears as though the adjuvant chemical was successful because all cells are vulnerable to the anti-cancer properties of the medication. Conversely, the presence of a third dimension in multicellular spheroids impedes the uptake of nutrients and treatments. Furthermore, certain cells, like those found in the *in vivo* TME, are in a heterogeneous proliferative state. This could lead to resistance since different cells in a 3D culture model are responsive to different drugs in different ways (Ncube et al., 2023). Advanced cell-based models, such as spheroids, are employed in various experimental contexts. However, more research is needed because the structure and biological properties of novel MDA-MB-231 TNBC spheroids have not yet been thoroughly characterised (Huang et al., 2020). Thus, there is a need to establish and characterise reliable and predictive platforms to improve drug screening and efficacy evaluation by considering the pathophysiology of the TME.

In our study, the novel doxorubicin-resistant MDA-MB-231 TNBC spheroid model was cultured and characterised for 27 days to assess its growth and viability. Spheroid growth and size are shown by planar surface area and soluble protein content (van Niekerk et al., 2023). The planar surface area and the protein values of the MDA-MB-231 DoxR TNBC spheroids demonstrated a clear correlation, where they increased almost linearly from day 11 to day 19. This is indicative of an increase in cell number. This was also observed visually in Figures 4.2 B and C. Both the protein values and planar surface area remained relatively stable until day 25. The decrease in the planar surface and protein content on day 27 and the decrease in observable spheroid size (Figure 4.2 F) suggested a decline in the model's viability at this particular time point.

In 2D and 3D cell cultures, intracellular ATP content is a commonly used technique to estimate the number of viable or metabolically active cells indirectly (van der Merwe et al., 2022). ATPases deplete the remaining ATP when cells lose viability and membrane integrity. Cell viability, physiological modifications brought on by treatment, and cellular stressors all have an impact on intracellular ATP concentrations (van Niekerk et al., 2023). AK is an enzyme found in the intermembrane gaps of the mitochondria. Transferring ATP energy from the mitochondria is essential, as it provides energy for cellular functions and maintains metabolic balance (Klepinin et al., 2020). AK is discharged from the mitochondria's intermembrane gaps once the integrity of the membrane is compromised as a result of cell death or other direct injury to the cells. This indicates a lack of membrane integrity (Calitz et al., 2018). Because these two parameters of cell viability have related roles, it is necessary to take into account how both interact when evaluating the cell viability of the model. During the characterisation of the MDA-MB-231 DoxR spheroid model, the measured ATP and AK were normalised per µg of protein. This addressed the variation in biomass brought about by the development or elimination of spheroids. Significant fluctuations in the ATP values between day 7 and day 9 suggested that the spheroids were still adjusting to their environment in the ClinoReactors™. The AK values increased from day 7 to day 9 but stabilised between day 15 and day 23 (Figure 4.3 (d)). The ATP values exhibited consistent, minimal fluctuations between days 15 and

23 (Figure 4.3 (c)), which is normal for ATP in spheroid models (van Niekerk et al., 2023) , indicating that metabolic equilibrium was reached at this time. Both ATP and AK values decreased on day 25 and increased on day 27. Cell death associated with apoptosis was suggested, with both ATP and AK levels being elevated on day 27. Glucose consumption increased from day 9 to day 11. From day 15, the glucose consumption stabilised until day 21 and then decreased from day 23 to day 27. Even when the glucose consumption decreased, the cells of the spheroids were still actively consuming glucose. Considering this data, the metabolically stable period, or the optimal experimental window for the MDA-MB-231 DoxR spheroids, was determined to be between day 15 and day 23 of culture (Figure 4.3 (b, c, d)).

Three treatment groups consisting of the doxorubicin and cisplatin clinical doses and the determined doxorubicin IC_{50} dose were used to assess the reactivity of the MDA-MB-231 DoxR spheroid model after daily treatment for 96 h. This was done to qualify the model for use as an assessment tool for treatments. Table 5.1 summarises the major findings following 96 h of treatment.

Table 5.1: Overview of normalised data for each treatment group after 96 h treatment with cisplatin clinical dose, doxorubicin clinical dose and doxorubicin [IC_{50}].

Sample treatment groups	Normalised average surface area per spheroid (μm^2)	Normalised soluble protein content per spheroid (µg)	Normalised ATP/Prot. values per soluble protein (µM/µg)	Normalised AK release per µg protein	Normalised glucose consumption per µg protein (mmol/L)
Untreated control	1	1	1	1	1
Cisplatin	0,72	0,17	1,39	8,87	0,55
Doxorubicin	0,91	0,37	4,54	3,67	0,71
Doxorubicin [IC_{50}]	0,72	0,40	0,14	6,21	1,87

The novel MDA-MB-231 DoxR spheroid model showed varying degrees of reactivity to all the treatments. The model was highly reactive to a clinical dose of cisplatin, as indicated by the reduction in spheroid size and integrity. The intracellular ATP and extracellular AK levels were evaluated to evaluate the treatments' cytotoxic effects. Adequate intracellular ATP levels are necessary for the process of apoptosis. In the event that ATP is depleted, cell death will occur, but necrosis will result (Eguchi et al., 1997). The model showed an increase in extracellular AK/protein content following treatment with cisplatin. There was also an increase in intracellular ATP/protein, which suggests that cisplatin resulted in apoptosis of the spheroids. The pronounced cytotoxic effects of cisplatin on the MDA-MB-231 were expected, as the cells had not previously been exposed to cisplatin.

The MDA-MB-231 DoxR spheroid model showed some level of resistance to the doxorubicin clinical dose, as indicated by a less pronounced reduction in spheroid size and integrity and a more moderate increase in extracellular AK/protein content. The clinical dose of doxorubicin also did not result in the same notable increase in intracellular ATP/protein content as observed with the other treatments (Figure 4.5 (c)).

The MDA-MB-231 DoxR spheroid model was also highly reactive to the determined IC_{50} dose of doxorubicin, as indicated by a significant reduction in spheroid size and an increase in extracellular AK/protein. There were also notable decreases in intracellular ATP/protein and approximate glucose consumption by the end of the treatment. The decrease in ATP and the increase in AK suggests that the doxorubicin IC_{50} resulted in necrosis of the spheroids after 96 h exposure (Figure 4.6 (c, d)). The loss of viability was comparable to that induced by the cisplatin treatment. The high level of toxicity of this treatment was to be expected as the dose was very high compared to the clinical dose of doxorubicin, although a greater measure of resistance was expected based on the resistance measured in the 2D cells.

There are two main ways that drug resistance in cancer can occur: acquired resistance and *de novo* resistance. Tumours can acquire resistance through alterations that occur during their exposure to therapies, while *de novo* resistance is linked to pre-therapy variables, including tumour cells adhering to the ECM (Lovitt et al., 2014). After repeated exposure of the 2D MDA-MB-231 cells to doxorubicin for nine months, the cells successfully acquired resistance, as determined by the MTT cytotoxicity assay. However, the resistant phenotype induced in 2D did not fully translate to 3D. Generally, it is considered that 3D cell-based models are usually more resistant because of their cell-cell and cell-ECM interactions, as well as their complex structure. However, it can be the inverse. Anti-cancer drugs have been shown in multiple studies to have effects on tumour cells in 3D cultures that are comparable to or greater than those of the identical tumour cell type grown in a 2D monolayer configuration (Lovitt et al., 2014), a similarity we see in our study. The difference between 2D and 3D drug response requires further elucidation. It could be that, when compared to cells grown in 2D monolayers, there may

be unobserved indirect effects on medication or chemical activity in tumour cells generated in 3D cultures. P-gp is a drug efflux transporter that triggers doxorubicin resistance (Mirzaei et al., 2022). The overexpression of this transporter results in enhanced drug efflux and reduces intracellular levels of chemotherapeutic agents (van Niekerk et al., 2023). It is possible that the potential drug-resistant mechanisms stimulated in 2D cell culture may be attributed to changes in the expression of genes encoding ABC transporter proteins, such as P-gp. This ABC transporter-linked resistance leading to drug efflux by means of P-gp, although unconfirmed, may not have fully translated to 3D.

The lack of resistance observed in this study may also be attributed to the 3D culture technique used, affecting the expression of ECM. Cells propagated as spheroids using different techniques show differential morphometric, diffusion, and chemo-sensitivity characteristics (Ncube et al., 2023). As previously mentioned, these techniques can be scaffold-based and scaffold-free. One substance that is frequently utilised in scaffold-based tissue engineering is scaffolds/ECM (Figure 5.1). This technique uses scaffolds such as hydrogels. Additionally, adaptable hydrogels can be made in a variety of ways, depending on the experiment being conducted. The cellular response to drugs is greatly influenced by cell-ECM protein interactions (Lovitt et al., 2018).

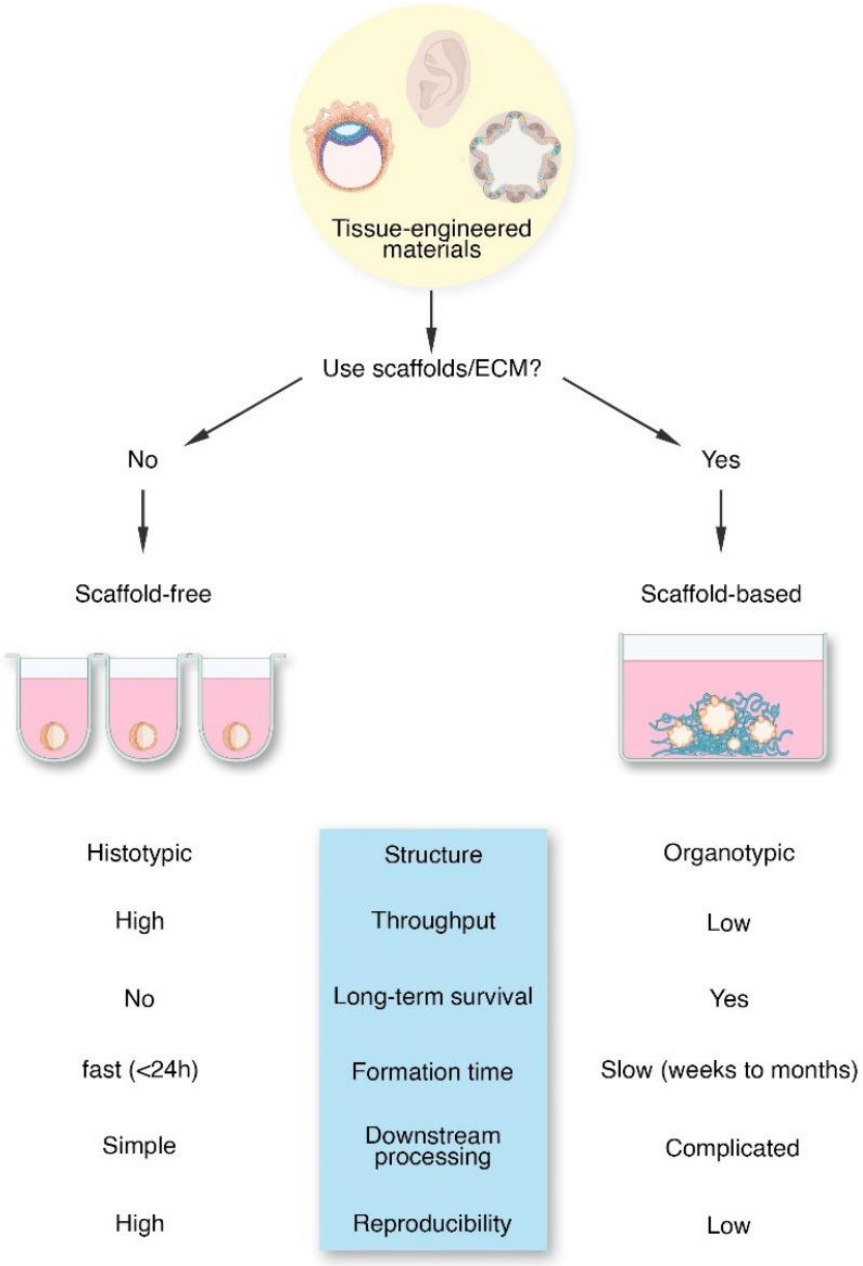

Figure 5.1: In tissue engineering, there are two primary approaches for creating three-dimensional cell aggregates, tissues, or organs based on the use of scaffolding materials like ECM and ECM-mimetic substances. Scaffold-free methods typically involve ultra-low adherent surfaces or techniques that induce the forced aggregation of cells into spheroids. In contrast, scaffold-based approaches utilise solid scaffolds (such as hydrogels, ECM, or synthetic polymers) to direct the formation of tissues or organs *in vitro* (Valdoz et al., 2021).

A study by Huang et al. 2020 used a scaffold-based technique (microwell array-agarose) to develop MDA-MB-231 spheroids. The results of the study showed that spheroids exhibited an increase in resistance to anti-cancer compounds, doxorubicin and carboplatin, an observation contradicting that obtained from this study. This discrepancy can be explained by the difference in the technique used to develop this model. The technique used in this study is a scaffold-free technique using a ClinoStar™ system with ClinoReactors™ to develop the MDA-MB-231 spheroid model. In contrast to the scaffold-based cultures, scaffold-free cultures initially do not have any association with ECM proteins (Figure 5.1), leading to cell death through anoikis (a certain type of apoptosis). It has been demonstrated that cultured scaffold-free spheroids secrete ECM proteins even though they are not supplied with exogenous ECM. However, ECM production can be affected, leading to low levels of ECM production. Certain cell types are sensitive to low ECM levels, which can lead to inhibited growth, senescence, and cell death (Valdoz et al., 2021). The attachment of cells to ECM proteins plays a role in mediating drug resistance (Lovitt et al., 2018). Additionally, Lovitt et al. 2018 investigated the impact of cell attachment to the ECM on cells grown in 3D cell culture with Matrigel and PuraMatrix, which promote spheroid formation in the absence of specific ECM proteins (e.g. laminin, collagen IV). Doxorubicin was applied to spheroids cultured on Matrigel and PuraMatrix, and comparisons of the cellular response were conducted. The potency of doxorubicin was significantly increased ($p \leq 0.05$) against the MDA-MB-231 cell line cultured in 3D on PuraMatrix when compared to Matrigel. Thus, the attachment of cells to selected ECM proteins may play a role in mediating drug resistance in MDA-MB-231 cells. Another study by Muranen et al. 2012 indicated that cellular attachment to the ECM permitted cell survival of ovarian cells cultured in 3D conditions upon exposure to BEZ235, an Akt/mammalian target of rapamycin (mTOR) inhibitor. Increased expression of Bcl-2 and Bcl-xL was detected in the cells situated at the periphery of the spheroid, specifically those in contact with the ECM. The study concluded that cell-ECM contacts can modulate anti-cancer activity (Muranen et al., 2012).

To further support the suggestion that the technique used could possibly influence drug resistance, a study by Qi et al. 2022 compared the drug resistance in scaffold-free and scaffold-based A549 spheroids. The results showed that resistance to chemotherapeutic drugs was higher in scaffold-based spheroids compared to scaffold-free spheroids. The study went on to state that a significant factor in the TME that plays a crucial role in drug resistance is ECM. In addition to the lack of pre-existing ECM, scaffold-free spheroids are capable of producing their own ECM. Simultaneously, scaffold-free spheroids deposited collagen l and laminin into the periphery, while scaffold-based spheroids generated greater levels of fibronectin, laminin, and collagen l. It is important to acknowledge that the overexpression of ECM components severely restricts the penetration of chemotherapeutic drugs. Thus, enhanced drug resistance can result from enhanced ECM production compared with their scaffold-free counterparts (Qi et al., 2022). The lack of significant resistance observed in this study could be attributed to the scaffold-free technique used to develop the MDA-MB-231 DoxR model.

CHAPTER SIX

6.0 CONCLUSION AND RECOMMENDATIONS

6.1 CONCLUSION

The established MDA-MB-231 DoxR spheroids were viable and functional and maintained their structure for at least 25 days. The data obtained from the various characterisation parameters indicated that the metabolically stable period was between days 15 and 23. Several significant advantages were realised by utilising the CelVivo ClinoStar™ system for developing the novel MDA-MB-231 DoxR spheroid model. The system ensured a highly consistent cell chamber volume, enabling accurate and uniform treatment per biomass, mimicking conditions closer to *in vivo* environments. Unlike some techniques, a specialised medium was unnecessary for culturing the spheroids. Temperature and gas exchange were carefully regulated in the ClinoReactors™, owing to the limited openings in the incubation system. This setup allowed for straightforward medium exchange and supported the execution of multiple assays because of the substantial yield of spheroids. The resulting spheroids were remarkably reproducible, uniform, and easy to sample (Wrzesinski et al., 2021). Physiologically, this technique is particularly relevant because it promotes the self-aggregation of cells to form spheroids, akin to natural tissue formation *in vivo*. Importantly, this scaffold-free approach allows spheroids to develop and grow in a natural microenvironment without the confounding effects of a scaffold. In contrast, scaffold-based techniques may create barriers around spheroids that potentially alter their drug resistance profiles, leading to less reliable results. Therefore, the method employed in this study offers enhanced physiological relevance by providing a more natural environment for spheroid growth and better reflecting *in vivo* conditions.

The 2D MDA-MB-231 cells acquired resistance following exposure to doxorubicin for nine months. However, even with the same resistant 2D MDA-MB-231 used to develop the 3D

MDA-MB-231 DoxR spheroid model, the spheroids did not show the same level of resistance to treatment but were instead sensitive to treatment with the chemotherapeutic compound. Even with resistance not being translated to the 3D MDA-MB-231 DoxR model in comparison to the 2D MDA-MB-231 cells, 3D cell-based models are still the better model. Unlike 2D cell-based models cultured on plastic substrates, culture flasks or Petri dishes, 3D cell-based models better mimic physiological conditions. Bioprocess forces, such as shear stress encountered during standard 2D cell culture, include hydrodynamic shear from flask shaking to aid detachment post-trypsinization, forces generated during centrifugation before cell pellet resuspension, and shear stress-induced during cell pellet resuspension via capillary transfer or pipetting. Culturing cells in these 2D conditions lacks physiological relevance and could lead to challenges in translating results to *in vivo* settings. Conversely, 3D cell-based models can be used to, at least partially, recreate the key components of a tumour, such as the architecture particular to the tissue and features in the surrounding microenvironment (Lovitt et al., 2014), thereby enhancing physiological relevance. Furthermore, given my results, it is evident that 2D and 3D cell-based models cannot be compared. Among 2D cell-based and 3D spheroid models, only 3D spheroid models demonstrate a drug response similar to that observed in solid tumours (Kapałczyńska et al., 2018).

The MDA-MB-231 DoxR spheroid model was highly sensitive to the doxorubicin IC_{50} when compared to the doxorubicin clinical dose, as the spheroids significantly decreased in size over the growth period and some spheroids lost their structural integrity (Figure 4.6 (f, C)), while the spheroids treated with the doxorubicin clinical dose maintained their structural integrity. Cell viability (ATP/protein) for the doxorubicin IC_{50}-treated spheroids was significantly affected as values decreased below those of the untreated control group. In contrast, cell viability for the doxorubicin clinical dose was not as affected: Values were above those of the untreated control group, and values increased after 72 h and 96 h of treatment after having declined at 48 h, which would suggest that the spheroids were trying to recover and becoming resistant to treatment. Regarding cell death, AK/protein values for the doxorubicin IC_{50} treated spheroids increased significantly between the first

24 h and 72 h of treatment, indicating that the treatment was killing the cells every time they were being treated. AK/protein values for the doxorubicin clinical dose-treated spheroids also increased. However, cell death was less significant than that observed in the doxorubicin IC_{50}-treatment group. Ultimately, it can be concluded that the MDA-MB-231 DoxR spheroid model is sensitive to a higher dose of doxorubicin and moderately resistant to a lower dose of doxorubicin. This model's responsiveness to different drug concentrations underscores its relevance in studying drug efficacy and resistance mechanisms in cancer treatment.

The cisplatin clinical dose treatment group results were comparable to those of the doxorubicin IC_{50} treatment group. The MDA-MB-231 DoxR spheroid model was also highly sensitive to cisplatin treatment. The degree of sensitivity to cisplatin treatment was to be expected, as the 2D cells used to develop the spheroids had not previously been exposed to cisplatin and had thus never acquired resistance to cisplatin. Many mechanisms can contribute to the lack of resistance to the chemotherapeutic compounds observed in the MDA-MB-231 DoxR spheroids. However, methods to investigate the alteration of physiological parameters within the 3D structures are currently limited. Many analytical methods that were originally designed to meet the requirements for monolayer culture evaluation fail to reveal the original biology of spheroids (Ncube et al., 2023).

Although this model does not appear useful as a resistant TNBC spheroid model, it may still be useful as a chemo-sensitive model for screening compounds for potential anti-cancer activity. Additional investigation of the dynamics of spheroid formation, the mechanisms of chemoresistance, and the therapeutic sensitivity to a broader range of antineoplastic drugs is required to characterise this model further.

Overall, these findings contribute to advancing our understanding of drug sensitivity and resistance in cancer cells within a more physiologically relevant 3D model. This knowledge is crucial for creating personalised cancer therapies and improving patient outcomes in clinical practice.

6.2 STUDY LIMITATIONS AND RECOMMENDATIONS

One of our limitations was adherence to the timeline apportioned for the studies. Due to insufficient time, we could not re-characterise and re-qualify our model to ensure reproducibility or correct all the experimental errors that could have affected our results. With sufficient finances and time, we could have performed a gene expression assay (qPCR) as a way to identify genes that may or may not have been expressed in our model to possibly explain the lack of resistance. A recovery period for our model to evaluate whether the spheroids would recover after treatment would have been beneficial as this would allow for more comprehensive conclusions about the resistance in the model. If the spheroids recovered following treatment, it could be concluded that they are resistant, and if the spheroids did not recover, it would have provided a more reliable conclusion of their lack of resistance. Furthermore, immunohistology assays to observe apoptosis and necrosis in the spheroids would have enhanced the findings.

Adding a fourth treatment group, one where the spheroids are developed using the sensitive 2D cells, could enable a comparison of the treatment reactivity between spheroids developed with the resistant 2D cells and the sensitive 2D cells. This comparison could possibly have led to a better understanding of the treatment reactivity of the MDA-MB-231 spheroids.

Spheroids are sensitive to handling, which may cause them to either clump together, become more compact, or break apart, thus resulting in variations in spheroid size and shape with continued handling. This variation in the size and shape of spheroids leads to large standard deviations, which can be observed in the 'Qualification of the MDA-MB-231 DoxR spheroid model treatment' figures.

VALUE OF THE STUDY

TNBC makes up 10 - 20% of all breast cancer cases diagnosed each year and is more common in younger women, particularly those of African ancestry (Nedeljković and Damjanović, 2019). TNBC is a complex disease because this type of breast cancer does not overexpress receptors, which makes targeted therapies difficult. It is the deadliest subtype of breast cancer due to its pronounced heterogeneity and aggressive behaviour, as well as the lack of treatment options. Cytotoxic chemotherapy and immune therapy remain the only available therapeutic strategies for treatment, but unfortunately, patients frequently develop resistance (Boichuk et al., 2017). In this study, we employed state-of-the-art technology that provides physiologically relevant research, with a reduction in the use of research animals. This has allowed us to develop a pre-clinical 3D TNBC cell-based model that closely resembles the complexities of the TME. The 3D spheroids, which were developed from 2D cell cultures, allowed us to study drug activity and compare the degree of chemo-sensitivity of 2D cultures versus 3D spheroids. The knowledge generated through this study will allow us to merge the gap between the in vitro breast cancer cellular profile and a tissue-based breast cancer profile, which is closer to an *in situ* profile.

FUNDING

This work is based on the research supported wholly / in part by the National Research Foundation of South Africa (Grant Number 138153).

REFERENCES

ABD EL-AZIZ, Y. S., SPILLANE, A. J., JANSSON, P. J. & SAHNI, S. 2021. Role of ABCB1 in mediating chemoresistance of triple-negative breast cancers. *Bioscience reports,* 41**,** BSR20204092.

ABDELAZIZ, A. G., NAGEH, H., ABDO, S. M., ABDALLA, M. S., AMER, A. A., ABDAL-HAY, A. & BARHOUM, A. 2023. A review of 3D polymeric scaffolds for bone tissue engineering: principles, fabrication techniques, immunomodulatory roles, and challenges. *Bioengineering,* 10**,** 204.

ABUWATFA, W. H., PITT, W. G. & HUSSEINI, G. A. 2024. Scaffold-based 3D cell culture models in cancer research. *Journal of Biomedical Science,* 31**,** 7.

AKRAM, M., IQBAL, M., DANIYAL, M. & KHAN, A. U. 2017. Awareness and current knowledge of breast cancer. *Biological research,* 50**,** 1-23.

ALFAROUK, K. O., STOCK, C.-M., TAYLOR, S., WALSH, M., MUDDATHIR, A. K., VERDUZCO, D., BASHIR, A. H., MOHAMMED, O. Y., ELHASSAN, G. O. & HARGUINDEY, S. 2015. Resistance to cancer chemotherapy: failure in drug response from ADME to P-gp. *Cancer cell international,* 15**,** 1-13.

ALGHUWAINEM, A., ALSHAREEDA, A. T. & ALSOWAYAN, B. 2019. Scaffold-free 3-D cell sheet technique bridges the gap between 2-D cell culture and animal models. *International journal of molecular sciences,* 20**,** 4926.

ANTONI, D., BURCKEL, H., JOSSET, E. & NOEL, G. 2015. Three-dimensional cell culture: a breakthrough in vivo. *International journal of molecular sciences,* 16**,** 5517-5527.

APARICIO, S., HIDALGO, M. & KUNG, A. L. 2015. Examining the utility of patient-derived xenograft mouse models. *Nature Reviews Cancer,* 15**,** 311-316.

AYATI, A., MOGHIMI, S., SALARINEJAD, S., SAFAVI, M., POURAMIRI, B. & FOROUMADI, A. 2020. A review on progression of epidermal growth factor receptor (EGFR) inhibitors as an efficient approach in cancer targeted therapy. *Bioorganic chemistry,* 99**,** 103811.

BADEA, M. A., BALAS, M. & DINISCHIOTU, A. 2022. Biological properties and development of hypoxia in a breast cancer 3D model generated by hanging drop technique. *Cell Biochemistry and Biophysics,* 80**,** 63-73.

BAI, X., NI, J., BERETOV, J., GRAHAM, P. & LI, Y. 2021. Triple-negative breast cancer therapeutic resistance: Where is the Achilles' heel? *Cancer letters,* 497**,** 100-111.

BELFIORE, L., AGHAEI, B., LAW, A. M., DOBROWOLSKI, J. C., RAFTERY, L. J., TJANDRA, A. D., YEE, C., PILONI, A., VOLKERLING, A. & FERRIS, C. J. 2021. Generation and analysis of 3D cell culture models for drug discovery. *European Journal of Pharmaceutical Sciences,* 163**,** 105876.

BENIEN, P. & SWAMI, A. 2014. 3D tumor models: history, advances and future perspectives. *Future oncology,* 10**,** 1311-1327.

BERGIN, A. R. & LOI, S. 2019. Triple-negative breast cancer: recent treatment advances. *F1000Research,* 8.

BIANCHINI, G., DE ANGELIS, C., LICATA, L. & GIANNI, L. 2022. Treatment landscape of triple-negative breast cancer—expanded options, evolving needs. *Nature reviews Clinical oncology,* 19**,** 91-113.

BOCA, I., CIUREA, A. I., CIORTEA, C. A. & DUDEA, S. M. 2021. Pros and cons for automated breast ultrasound (ABUS): a narrative review. *Journal of Personalized Medicine,* 11**,** 703.

BOICHUK, S., GALEMBIKOVA, A., SITENKOV, A., KHUSNUTDINOV, R., DUNAEV, P., VALEEVA, E. & USOLOVA, N. 2017. Establishment and characterization of a triple negative basal-like breast cancer cell line with multi-drug resistance. *Oncology letters,* 14**,** 5039-5045.

BONORA, M., PATERGNANI, S., RIMESSI, A., DE MARCHI, E., SUSKI, J. M., BONONI, A., GIORGI, C., MARCHI, S., MISSIROLI, S. & POLETTI, F. 2012. ATP synthesis and storage. *Purinergic signalling,* 8**,** 343-357.

BRANCATO, V., OLIVEIRA, J. M., CORRELO, V. M., REIS, R. L. & KUNDU, S. C. 2020. Could 3D models of cancer enhance drug screening? *Biomaterials,* 232**,** 119744.

CALITZ, C., HAMMAN, J. H., VILJOEN, A. M., FEY, S. J., WRZESINSKI, K. & GOUWS, C. 2018. Toxicity and anti-prolific properties of Xysmalobium undulatum water extract during short-term exposure to two-dimensional and three-dimensional spheroid cell cultures. *Toxicology mechanisms and methods,* 28**,** 641-652.

CARMELIET, P. & JAIN, R. K. 2011. Molecular mechanisms and clinical applications of angiogenesis. *Nature,* 473**,** 298-307.

CHAICHAROENAUDOMRUNG, N., KUNHORM, P. & NOISA, P. 2019. Three-dimensional cell culture systems as an in vitro platform for cancer and stem cell modeling. *World journal of stem cells,* 11**,** 1065.

COHEN, S. Y., STOLL, C. R., ANANDARAJAH, A., DOERING, M. & COLDITZ, G. A. 2023. Modifiable risk factors in women at high risk of breast cancer: a systematic review. *Breast Cancer Research,* 25**,** 45.

COLEMAN, C. Early detection and screening for breast cancer. Seminars in oncology nursing, 2017. Elsevier, 141-155.

COLLIGNON, J., LOUSBERG, L., SCHROEDER, H. & JERUSALEM, G. 2016. Triple-negative breast cancer: treatment challenges and solutions. *Breast Cancer: Targets and Therapy***,** 93-107.

COOPER, G. M. & HAUSMAN, R. 2000. A molecular approach. *The Cell. 2nd ed. Sunderland, MA: Sinauer Associates***,** 1394-403.

DEWI, T. K., RUITER, R. A., ARDI, R. & MASSAR, K. 2022. The role of psychosocial variables in breast self-examination practice: Results from focus group discussions in Surabaya, Indonesia. *Psycho-Oncology,* 31**,** 1169-1177.

DUDA, K., MAJERCZAK, J., NIECKARZ, Z., HEYMSFIELD, S. B. & ZOLADZ, J. A. 2019. Human body composition and muscle mass. *Muscle and exercise physiology.* Elsevier.

EDMONDSON, R., BROGLIE, J. J., ADCOCK, A. F. & YANG, L. 2014. Three-dimensional cell culture systems and their applications in drug discovery and cell-based biosensors. *Assay and drug development technologies,* 12**,** 207-218.

EGELSTON, C. A., GUO, W., YOST, S. E., GE, X., LEE, J. S., FRANKEL, P. H., CUI, Y., RUEL, C., SCHMOLZE, D. & MURGA, M. 2023. Immunogenicity and efficacy of pembrolizumab and doxorubicin in a phase I trial for patients with metastatic triple-negative breast cancer. *Cancer Immunology, Immunotherapy,* 72**,** 3013-3027.

EGUCHI, Y., SHIMIZU, S. & TSUJIMOTO, Y. 1997. Intracellular ATP levels determine cell death fate by apoptosis or necrosis. *Cancer research,* 57**,** 1835-1840.

ENGEBRAATEN, O., VOLLAN, H. K. M. & BøRRESEN-DALE, A.-L. 2013. Triple-negative breast cancer and the need for new therapeutic targets. *The American journal of pathology,* 183**,** 1064-1074.

FEY, S. J. & WRZESINSKI, K. 2012. Determination of drug toxicity using 3D spheroids constructed from an immortal human hepatocyte cell line. *Toxicological sciences,* 127**,** 403-411.

FIRATLIGIL-YILDIRIR, B. & YALCIN-OZUYSAL, O. 2023. Recent advances in lab-on-a-chip systems for breast cancer metastasis research. *Nanoscale Advances,* 5**,** 2375-2393.

FOLKMAN, J. Role of angiogenesis in tumor growth and metastasis. Seminars in oncology, 2002. Elsevier, 15-18.

FONTANA, F., RAIMONDI, M., MARZAGALLI, M., SOMMARIVA, M., GAGLIANO, N. & LIMONTA, P. 2020. Three-dimensional cell cultures as an in vitro tool for prostate cancer modeling and drug discovery. *International journal of molecular sciences,* 21**,** 6806.

FRANCO, Y. L., VAIDYA, T. R. & AIT-OUDHIA, S. 2018. Anticancer and cardio-protective effects of liposomal doxorubicin in the treatment of breast cancer. *Breast Cancer: Targets and Therapy***,** 131-141.

GALOGRE, M., RODIN, D., PYATNITSKIY, M., MACKELPRANG, M. & KOMAN, I. 2023. A review of HER2 overexpression and somatic mutations in cancers. *Critical Reviews in Oncology/Hematology,* 186**,** 103997.

GAO, Y., MOY, L. & HELLER, S. L. 2021a. Digital breast tomosynthesis: update on technology, evidence, and clinical practice. *Radiographics,* 41**,** 321-337.

GAO, Y., REIG, B., HEACOCK, L., BENNETT, D. L., HELLER, S. L. & MOY, L. 2021b. Magnetic resonance imaging in screening of breast cancer. *Radiologic Clinics,* 59**,** 85-98.

GARLAPATI, C., JOSHI, S., SAHOO, B., KAPOOR, S. & ANEJA, R. 2019. The persisting puzzle of racial disparity in triple negative breast cancer: looking through a new lens. *Frontiers in Bioscience-Scholar,* 11**,** 75-88.

GHASEMI, M., TURNBULL, T., SEBASTIAN, S. & KEMPSON, I. 2021. The MTT assay: utility, limitations, pitfalls, and interpretation in bulk and single-cell analysis. *International journal of molecular sciences,* 22**,** 12827.

GóMEZ-OLIVA, R., DOMíNGUEZ-GARCíA, S., CARRASCAL, L., ABALOS-MARTíNEZ, J., PARDILLO-DíAZ, R., VERáSTEGUI, C., CASTRO, C., NUNEZ-ABADES, P. & GERIBALDI-DOLDáN, N. 2021. Evolution of experimental models in the study of glioblastoma: toward finding efficient treatments. *Frontiers in oncology,* 10**,** 614295.

GOUWS, C., SMIT, T., WILLERS, C., SVITINA, H., CALITZ, C. & WRZESINSKI, K. 2021. Anticancer potential of Sutherlandia frutescens and Xysmalobium undulatum in LS180 colorectal cancer mini-tumors. *Molecules,* 26**,** 605.

GUERRERO, V. G., BAEZ, A. F., COFRé GONZáLEZ, C. G. & MIñO GONZáLEZ, C. G. 2017. Monitoring modifiable risk factors for breast cancer: an obligation for health professionals. *Revista Panamericana de Salud Pública,* 41**,** e80.

GUESTINI, F., ONO, K., MIYASHITA, M., ISHIDA, T., OHUCHI, N., NAKAGAWA, S., HIRAKAWA, H., TAMAKI, K., OHI, Y. & RAI, Y. 2019. Impact of Topoisomerase IIα, PTEN, ABCC1/MRP1, and KI67 on triple-negative breast cancer patients treated with neoadjuvant chemotherapy. *Breast cancer research and treatment,* 173**,** 275-288.

HALL, M. D., MARTIN, C., FERGUSON, D. J., PHILLIPS, R. M., HAMBLEY, T. W. & CALLAGHAN, R. 2004. Comparative efficacy of novel platinum (IV) compounds with established chemotherapeutic drugs in solid tumour models. *Biochemical pharmacology,* 67**,** 17-30.

HANAHAN, D. 2022. Hallmarks of cancer: new dimensions. *Cancer discovery,* 12**,** 31-46.

HANAHAN, D. & WEINBERG, R. A. 2011. Hallmarks of cancer: the next generation. *cell,* 144**,** 646-674.

HANAHAN, D. & WEINBERG, R. A. 2017. Biological hallmarks of cancer. *Holland-Frei Cancer Medicine,* 1**,** 1-10.

HARLEY, C. B., FUTCHER, A. B. & GREIDER, C. W. 1990. Telomeres shorten during ageing of human fibroblasts. *Nature,* 345**,** 458-460.

HE, L., WICK, N., GERMANS, S. K. & PENG, Y. 2021. The role of breast cancer stem cells in chemoresistance and metastasis in triple-negative breast cancer. *Cancers,* 13**,** 6209.

HUANG, N., CHEN, L., HE, J. & NGUYEN, Q. D. 2022. The efficacy of clinical breast exams and breast self-exams in detecting malignancy or positive ultrasound findings. *Cureus,* 14.

HUANG, Z., YU, P. & TANG, J. 2020. Characterization of triple-negative breast cancer MDA-MB-231 cell spheroid model. *OncoTargets and therapy***,** 5395-5405.

IQBAL, N. & IQBAL, N. 2014. Human epidermal growth factor receptor 2 (HER2) in cancers: overexpression and therapeutic implications. *Molecular biology international,* 2014**,** 852748.

JAFRI, M. A., ANSARI, S. A., ALQAHTANI, M. H. & SHAY, J. W. 2016. Roles of telomeres and telomerase in cancer, and advances in telomerase-targeted therapies. *Genome medicine,* 8**,** 1-18.

JENSEN, C. & TENG, Y. 2020. Is it time to start transitioning from 2D to 3D cell culture? *Frontiers in molecular biosciences,* 7**,** 33.

JOHNSON-ARBOR, K. & DUBEY, R. 2017. Doxorubicin.

JUBELIN, C., MUñOZ-GARCIA, J., GRISCOM, L., COCHONNEAU, D., OLLIVIER, E., HEYMANN, M.-F., VALLETTE, F. M., OLIVER, L. & HEYMANN, D. 2022. Three-dimensional in vitro culture models in oncology research. *Cell & Bioscience,* 12**,** 155.

KAPAŁCZYńSKA, M., KOLENDA, T., PRZYBYłA, W., ZAJąCZKOWSKA, M., TERESIAK, A., FILAS, V., IBBS, M., BLIźNIAK, R., ŁUCZEWSKI, Ł. & LAMPERSKA, K. 2018. 2D and 3D cell cultures–a comparison of different types of cancer cell cultures. *Archives of medical science,* 14**,** 910-919.

KITAEVA, K. V., RUTLAND, C. S., RIZVANOV, A. A. & SOLOVYEVA, V. V. 2020. Cell culture based in vitro test systems for anticancer drug screening. *Frontiers in Bioengineering and Biotechnology,* 8**,** 322.
KLEPININ, A., ZHANG, S., KLEPININA, L., REBANE-KLEMM, E., TERZIC, A., KAAMBRE, T. & DZEJA, P. 2020. Adenylate kinase and metabolic signaling in cancer cells. *Frontiers in oncology,* 10**,** 660.
LAMBERT, A. W., PATTABIRAMAN, D. R. & WEINBERG, R. A. 2017. Emerging biological principles of metastasis. *Cell,* 168**,** 670-691.
LANGHANS, S. A. 2018. Three-dimensional in vitro cell culture models in drug discovery and drug repositioning. *Frontiers in pharmacology,* 9**,** 6.
LEHMANN, B. D., PIETENPOL, J. A. & TAN, A. R. 2015. Triple-negative breast cancer: molecular subtypes and new targets for therapy. *American Society of Clinical Oncology Educational Book,* 35**,** e31-e39.
LIMA, S. M., KEHM, R. D. & TERRY, M. B. 2021. Global breast cancer incidence and mortality trends by region, age-groups, and fertility patterns. *EClinicalMedicine,* 38.
LOH, Q. L. & CHOONG, C. 2013. Three-dimensional scaffolds for tissue engineering applications: role of porosity and pore size.
LOVITT, C. J., SHELPER, T. B. & AVERY, V. M. 2014. Advanced cell culture techniques for cancer drug discovery. *Biology,* 3**,** 345-367.
LOVITT, C. J., SHELPER, T. B. & AVERY, V. M. 2018. Doxorubicin resistance in breast cancer cells is mediated by extracellular matrix proteins. *BMC cancer,* 18**,** 1-11.
MA, W.-Y., HSIUNG, L.-C., WANG, C.-H., CHIANG, C.-L., LIN, C.-H., HUANG, C.-S. & WO, A. M. 2015. A novel 96well-formatted micro-gap plate enabling drug response profiling on primary tumour samples. *Scientific reports,* 5**,** 9656.
MANDAPATI, A. & LUKONG, K. E. 2023. Triple negative breast cancer: Approved treatment options and their mechanisms of action. *Journal of cancer research and clinical oncology,* 149**,** 3701-3719.
MARRA, A., TRAPANI, D., VIALE, G., CRISCITIELLO, C. & CURIGLIANO, G. 2020. Practical classification of triple-negative breast cancer: intratumoral heterogeneity, mechanisms of drug resistance, and novel therapies. *NPJ breast cancer,* 6**,** 54.
MCCLATCHEY, A. I. & YAP, A. S. 2012. Contact inhibition (of proliferation) redux. *Current opinion in cell biology,* 24**,** 685-694.
MCDERMOTT, M., EUSTACE, A. J., BUSSCHOTS, S., BREEN, L., CROWN, J., CLYNES, M., O'DONOVAN, N. & STORDAL, B. 2014. In vitro development of chemotherapy and targeted therapy drug-resistant cancer cell lines: a practical guide with case studies. *Frontiers in oncology,* 4**,** 40.
MIRZAEI, S., GHOLAMI, M. H., HASHEMI, F., ZABOLIAN, A., FARAHANI, M. V., HUSHMANDI, K., ZARRABI, A., GOLDMAN, A., ASHRAFIZADEH, M. & ORIVE, G. 2022. Advances in understanding the role of P-gp in doxorubicin resistance: Molecular pathways, therapeutic strategies, and prospects. *Drug Discovery Today,* 27**,** 436-455.
MOSKOWITZ, C. S., RONCKERS, C. M., CHOU, J. F., SMITH, S. A., FRIEDMAN, D. N., BARNEA, D., KOK, J. L., DE VRIES, S., WOLDEN, S. L. & HENDERSON, T. O. 2021.

Development and validation of a breast cancer risk prediction model for childhood cancer survivors treated with chest radiation: a report from the Childhood Cancer Survivor Study and the Dutch Hodgkin late effects and LATER cohorts. *Journal of Clinical Oncology,* 39**,** 3012-3021.

MUñOZ-ESPíN, D. & SERRANO, M. 2014. Cellular senescence: from physiology to pathology. *Nature reviews Molecular cell biology,* 15**,** 482-496.

MURANEN, T., SELFORS, L. M., WORSTER, D. T., IWANICKI, M. P., SONG, L., MORALES, F. C., GAO, S., MILLS, G. B. & BRUGGE, J. S. 2012. Inhibition of PI3K/mTOR leads to adaptive resistance in matrix-attached cancer cells. *Cancer cell,* 21**,** 227-239.

MURPHY, S. V. & ATALA, A. 2014. 3D bioprinting of tissues and organs. *Nature biotechnology,* 32**,** 773-785.

NCUBE, K. N., JURGENS, T., STEENKAMP, V., CROMARTY, A. D., VAN DEN BOUT, I. & CORDIER, W. 2023. Comparative evaluation of the cytotoxicity of Doxorubicin in BT-20 triple-negative breast carcinoma monolayer and spheroid cultures. *Biomedicines,* 11**,** 1484.

NEDELJKOVIć, M. & DAMJANOVIć, A. 2019. Mechanisms of chemotherapy resistance in triple-negative breast cancer—how we can rise to the challenge. *Cells,* 8**,** 957.

NYGA, A., CHEEMA, U. & LOIZIDOU, M. 2011. 3D tumour models: novel in vitro approaches to cancer studies. *Journal of cell communication and signaling,* 5**,** 239-248.

PARK, Y., HUH, K. M. & KANG, S.-W. 2021. Applications of biomaterials in 3D cell culture and contributions of 3D cell culture to drug development and basic biomedical research. *International Journal of Molecular Sciences,* 22**,** 2491.

PINTO, B., HENRIQUES, A. C., SILVA, P. M. & BOUSBAA, H. 2020. Three-dimensional spheroids as in vitro preclinical models for cancer research. *Pharmaceutics,* 12**,** 1186.

POLK, A., SVANE, I.-M., ANDERSSON, M. & NIELSEN, D. 2018. Checkpoint inhibitors in breast cancer–current status. *Cancer treatment reviews,* 63**,** 122-134.

POZZI, S., SCOMPARIN, A., DANGOOR, S. I., AJAMIL, D. R., OFEK, P., NEUFELD, L., KRIVITSKY, A., VASKOVICH-KOUBI, D., KLEINER, R. & DEY, P. 2021. Meet me halfway: Are in vitro 3D cancer models on the way to replace in vivo models for nanomedicine development? *Advanced Drug Delivery Reviews,* 175**,** 113760.

QI, X., PROKHOROVA, A. V., MEZENTSEV, A. V., SHEN, N., TROFIMENKO, A. V., FILKOV, G. I., SULIMANOV, R. A., MAKAROV, V. A. & DURYMANOV, M. O. 2022. Comparison of EMT-related and multi-drug resistant gene expression, extracellular matrix production, and drug sensitivity in NSCLC spheroids generated by scaffold-free and scaffold-based methods. *International Journal of Molecular Sciences,* 23**,** 13306.

RABANEL, J.-M., BERTRAND, N., SANT, S., LOUATI, S. & HILDGEN, P. 2006. Polysaccharide hydrogels for the preparation of immunoisolated cell delivery systems. ACS Publications.

RADTKE, A. L. & HERBST-KRALOVETZ, M. M. 2012. Culturing and applications of rotating wall vessel bioreactor derived 3D epithelial cell models. *JoVE (Journal of Visualized Experiments)***,** e3868.

REEVES, R. A. & KAUFMAN, T. 2020. Mammography.
ROARTY, K. & ECHEVERRIA, G. V. 2021. Laboratory models for investigating breast cancer therapy resistance and metastasis. *Frontiers in oncology,* 11**,** 645698.
RODLER, E., SHARMA, P., BARLOW, W. E., GRALOW, J. R., PUHALLA, S. L., ANDERS, C. K., GOLDSTEIN, L., TRIPATHY, D., BROWN-GLABERMAN, U. A. & HUYNH, T.-T. 2023. Cisplatin with veliparib or placebo in metastatic triple-negative breast cancer and BRCA mutation-associated breast cancer (S1416): a randomised, double-blind, placebo-controlled, phase 2 trial. *The lancet oncology,* 24**,** 162-174.
ROGNE, P., ROSSELIN, M., GRUNDSTRöM, C., HEDBERG, C., SAUER, U. H. & WOLF-WATZ, M. 2018. Molecular mechanism of ATP versus GTP selectivity of adenylate kinase. *Proceedings of the National Academy of Sciences,* 115**,** 3012-3017.
RYAN, S.-L., BAIRD, A.-M., VAZ, G., URQUHART, A. J., SENGE, H., RICHARD, D. J., O'BYRNE, K. J. & DAVIES, A. M. 2016. Drug discovery approaches utilizing three-dimensional cell culture. *Assay and drug development technologies,* 14**,** 19-28.
RYU, N.-E., LEE, S.-H. & PARK, H. 2019. Spheroid culture system methods and applications for mesenchymal stem cells. *Cells,* 8**,** 1620.
SABBAH, D. A., HAJJO, R. & SWEIDAN, K. 2020. Review on epidermal growth factor receptor (EGFR) structure, signaling pathways, interactions, and recent updates of EGFR inhibitors. *Current topics in medicinal chemistry*.
SARASWATHY, M. & GONG, S. 2013. Different strategies to overcome multidrug resistance in cancer. *Biotechnology advances,* 31**,** 1397-1407.
SEVER, R. & BRUGGE, J. S. 2015. Signal transduction in cancer. *Cold Spring Harbor perspectives in medicine,* 5**,** a006098.
SHIOVITZ, S. & KORDE, L. A. 2015. Genetics of breast cancer: a topic in evolution. *Annals of Oncology,* 26**,** 1291-1299.
SIERRA, M. A., WHEELER, J. C., DEVEREUX, L., TRAINER, A. H. & KEOGH, L. 2021. Exploring implementation of personal breast cancer risk assessments. *Journal of Personalized Medicine,* 11**,** 992.
SMIT, T., CALITZ, C., WILLERS, C., SVITINA, H., HAMMAN, J., FEY, S. J., GOUWS, C. & WRZESINSKI, K. 2020. Characterization of an alginate encapsulated LS180 spheroid model for anti-colorectal cancer compound screening. *ACS medicinal chemistry letters,* 11**,** 1014-1021.
SUN, Y.-S., ZHAO, Z., YANG, Z.-N., XU, F., LU, H.-J., ZHU, Z.-Y., SHI, W., JIANG, J., YAO, P.-P. & ZHU, H.-P. 2017. Risk factors and preventions of breast cancer. *International journal of biological sciences,* 13**,** 1387.
SUNG, H., FERLAY, J., SIEGEL, R. L., LAVERSANNE, M., SOERJOMATARAM, I., JEMAL, A. & BRAY, F. 2021. Global cancer statistics 2020: GLOBOCAN estimates of incidence and mortality worldwide for 36 cancers in 185 countries. *CA: a cancer journal for clinicians,* 71**,** 209-249.
SZNURKOWSKA, M. K. & ACETO, N. 2022. The gate to metastasis: key players in cancer cell intravasation. *The FEBS journal,* 289**,** 4336-4354.
TAN, D. & DAYU, A. 2022. Menopausal hormone therapy: why we should no longer be afraid of the breast cancer risk. *Climacteric,* 25**,** 362-368.

THOMA, C. R., ZIMMERMANN, M., AGARKOVA, I., KELM, J. M. & KREK, W. 2014. 3D cell culture systems modeling tumor growth determinants in cancer target discovery. *Advanced drug delivery reviews,* 69**,** 29-41.

TIMM, D. M., CHEN, J., SING, D., GAGE, J. A., HAISLER, W. L., NEELEY, S. K., RAPHAEL, R. M., DEHGHANI, M., ROSENBLATT, K. P. & KILLIAN, T. 2013. A high-throughput three-dimensional cell migration assay for toxicity screening with mobile device-based macroscopic image analysis. *Scientific reports,* 3**,** 3000.

VALASTYAN, S. & WEINBERG, R. A. 2011. Tumor metastasis: molecular insights and evolving paradigms. *Cell,* 147**,** 275-292.

VALDOZ, J. C., JOHNSON, B. C., JACOBS, D. J., FRANKS, N. A., DODSON, E. L., SANDERS, C., CRIBBS, C. G. & VAN RY, P. M. 2021. The ECM: to scaffold, or not to scaffold, that is the question. *International Journal of Molecular Sciences,* 22**,** 12690.

VAN DER MERWE, L., SVITINA, H., WILLERS, C., WRZESINSKI, K. & GOUWS, C. 2022. A novel NCI-H69V small cell lung cancer functional mini-tumor model for future treatment screening applications. *Biotechnology Progress,* 38**,** e3253.

VAN NIEKERK, A., WRZESINSKI, K., STEYN, D. & GOUWS, C. 2023. A novel NCI-H69AR drug-resistant small-cell lung cancer mini-tumor model for anti-cancer treatment screening. *Cells,* 12**,** 1980.

VTORUSHIN, S., DULESOVA, A. & KRAKHMAL, N. 2022. Luminal androgen receptor (LAR) subtype of triple-negative breast cancer: molecular, morphological, and clinical features. *Journal of Zhejiang University-SCIENCE B,* 23**,** 617-624.

WANIGASEKARA, J., CULLEN, P. J., BOURKE, P., TIWARI, B. & CURTIN, J. F. 2023. Advances in 3D culture systems for therapeutic discovery and development in brain cancer. *Drug Discovery Today,* 28**,** 103426.

WEINBERG, R. & HANAHAN, D. 2000. The hallmarks of cancer. *Cell,* 100**,** 57-70.

WON, K. A. & SPRUCK, C. 2020. Triple-negative breast cancer therapy: Current and future perspectives. *International journal of oncology,* 57**,** 1245-1261.

WRZESINSKI, K., ALNøE, S., JOCHUMSEN, H. H., MIKKELSEN, K., BRYLD, T. D., VISTISEN, J. S., ALNøE, P. W. & FEY, S. J. 2021. A Purpose-Built System for Culturing Cells as In Vivo Mimetic 3D Structures. *Biomechanics and Functional Tissue Engineering.* IntechOpen.

YIN, L., DUAN, J.-J., BIAN, X.-W. & YU, S.-C. 2020. Triple-negative breast cancer molecular subtyping and treatment progress. *Breast Cancer Research,* 22**,** 1-13.

ZHU, Y., YANG, R., LAW, J. H., KHAN, M., YIP, K. W. & SUN, Q. 2022. Hallmark of cancer: Resisting cell death. Frontiers Media SA.

APPENDIX 1

DocuSign Envelope ID: FB864811-9809-4F3E-8498-7EACACCE185F

Royal Society of Chemistry
Thomas Graham House
Science Park
Milton Road
Cambridge
CB4 0WF

Tel: +44 (0)1223 420 066

www.rsc.org

25 June 2024

To Viwe Fokazi

The Royal Society of Chemistry (RSC) hereby grants permission for the use of the material specified below in the printed and microfilm version of your thesis, and as part of your thesis in your university's digital repository.

Permission is granted as long as the articles are fully acknowledged and a link is given back to the articles on our Platform. Please go to rsc.li/permissions for details. Please note that if the material specified above or any part of it appears with credit or acknowledgement to a third party then you must also secure permission from that third party before reproducing that material.

The related article is:

Recent advances in lab-on-a-chip systems for breast cancer metastasis research
Burcu Firatligil-Yildirir, Ozden Yalcin-Ozuysal and Nonappa
Nanoscale Adv., 2023,**5**, 2375-2393

Material for reuse:
Figure 1

Yours sincerely

DocuSigned by:
Becky Roberts
C0B8BD4FBFD54CA...

Becky Roberts
Contracts & Copyright Executive
Royal Society of Chemistry

APPENDIX 2

UNIVERSITY OF THE FREE STATE
UNIVERSITEIT VAN DIE VRYSTAAT
YUNIVESITHI YA FREISTATA

UFS·UV
RESEARCH DEVELOPMENT
NAVORSINGSONTWIKKELING

Environment & Biosafety Research Ethics Committee

09-Feb-2023

Dear **Viwe Fokazi**

Project Title: **Establishing a doxorubicin-resistant triple negative breast cancer spheroid model**

Department: **Pharmacology Department (Bloemfontein Campus)**

APPLICATION APPROVED

This letter confirms that this research proposal was given ethical clearance by the Environment & Biosafety Research Ethics Committee of the University of the Free State.

Your ethical clearance number, to be used in all correspondence is: **UFS-ESD2022/0303**

Please note the following:

1. **This ethical clearance is valid for two years from the issuance of this letter.**
2. **If the research takes longer than two years to complete, please submit a Continuation Report to the Ethics Committee before ethical clearance expires.**
3. **If any changes are made during the research process (including a change in investigators), please inform the Ethics Committee by submitting an Amendment.**
4. **When the research is concluded, please submit a Final Report to the Ethics Committee.**

Thank you for your application and we wish you well in all of your research endeavours.

Yours Sincerely

Prof. RR (Robert) Bragg
Chairperson: Environment & Biosafety Research Ethics Committee
University of the Free State

Directorate: Research Development
T: +27 (0)51 401 9398 | +27 (0)51 401 2075 | E: smitham@ufs.ac.za
Johannes Brill Building, Room 106D, First Floor
205 Nelson Mandela Drive | Park West, Bloemfontein 9301 | South Africa
P.O. Box 339 | Bloemfontein 9300 | South Africa | www.ufs.ac.za

APPENDIX 3

ETHEL ROSS

English language editing and proofreading

22 July 2024

To whomever it may concern:

This letter serves to confirm that I worked as the proofreader and language editor on Viwe Fokazi's (student 2019374566) Master's thesis:

Establishing a doxorubicin-resistant triple-negative breast cancer spheroid model

In no way did I change the content.

Yours faithfully

Ethel Ross (BA Hons; H Dip Ed)

Email: clanross1@icon.co.za Tel: 083 954 5412